MILLI ROBOTICS FOR ENDOSCOPY

by

Jeff Wendlandt

Memorandum No. UCB/ERL M94/7

16 February 1994

MILLI ROBOTICS FOR ENDOSCOPY

by

Jeff Wendlandt

Memorandum No. UCB/ERL M94/7

16 February 1994

ELECTRONICS RESEARCH LABORATORY

College of Engineering
University of California, Berkeley
94720

MILLI ROBOTICS FOR ENDOSCOPY

by

Jeff Wendlandt

Memorandum No. UCB/ERL M94/7

16 February 1994

ELECTRONICS RESEARCH LABORATORY

College of Engineering
University of California, Berkeley
94720

Abstract

Endoscopy is a minimally invasive surgical technique used to examine and operate in the gastrointestinal tract. Current instruments lack fine motion control and dexterity. This report proposes solutions to remedy the problem by designing new equipment or modifying existing equipment. A background in endoscopy is presented along with an explanation of the problems experienced by surgeons. The report then describes concept design solutions to the problems described. A tendon driven manipulator is described in detail. The kinematics and dynamics are explored as well as the control of the device. This tendon driven device differs from many tendon driven devices in that the number of degrees of freedom equals the number of tendons. Simulation results for the manipulator are given as well a brief description of the prototype.

Contents

1 Introduction

This report describes work in designing new tools and equipment for endoscopy. Endoscopy is a minimally invasive surgical technique which performs operations and inspections in the gastrointestinal tract. Endoscopy's primary benefit is that it allows the patient to recover much more quickly then conventional surgery. Some patients can not withstand major surgery but can withstand the procedures performed in endoscopy. Endoscopy can extend the patients life in these cases. Major improvements have been made in endoscopy by providing clearer images of the interior of the patient. Electronic video endoscopes are improving and are more popular than fiberoptic scopes according to [10]. There have been attempts to improve the mechanical function of the endoscope and the tools. An endoscopic suturing device is described in [6]. Some researchers propose modifying the entire endoscope as in [17] and [9]. It is the belief of this author that a primary failure of current endoscopic instruments is the lack of the ability to perform fine motion control. Without it, tasks take longer than necessary and accuracy is lost. Time can be saved by using better tools. This report first gives a background of endoscopy and describes the procedures and tools used. The limitations of the tools are discussed. Problems that endoscopists experience are described. Several concept designs are introduced to remedy the problems experienced by surgeons. A particular design is discussed in detail. It is a tendon controlled device which allows general fine motion control of current endoscopic tools. The actuation is provided through small cables. This device varies from many other tendon controlled devices since it has the same number of tendons as degrees of freedom. A kinematic as well as a dynamic analysis is performed and described. The kinematic and dynamic analysis were aided by the use of a mathematic symbolic software tool. A controller is developed and the controlled system is simulated. The report finishes with a brief presentation of a prototype of the tendon controlled device. This report primarily intends to develop better instruments for endoscopy by modifying the current tools or by designing new ones.

2 Endoscopes and Accessories

Most of the background on endoscopes and the accessories discussed in this section is provided in [1]. Modern flexible endoscopes are typically variations on the same design shown in Figure 1. The endoscope consists of a headset connected to a long flexible tube which is inserted into the body. The headset holds buttons for controlling the video options, suction, air, and water. Video options include freezing a frame, storing a frame, and creating additional windows. The control dials for the tip of the endoscope are located on the headset. There are two concentric dials which control the up-down direction and the left-right direction. Each dial can be individually fixed by a locking lever. The light source is attached to a tube which is attached to the headset. The light is then transmitted to the end of the endoscope through a fiberoptic bundle. The tools used in endoscopy are inserted through the tool channel located at the base of the headset. The tool channel is located in the flexible

tube and exits at the tip. The flexible tube is attached to the end of the headset. The length of the flexible tube varies between 70 − 110 cm for 'short' endoscopes and 165 − 180 cm for 'long' endoscopes [1]. The flexible tube contains a tool channel, one or two light sources, a lens for the optics and one or two air/water channels. The inner diameters of tool channels range between 2.8 mm and 5.5 mm. The typical inner diameter of tool channels is 2.8 mm. The typical outer diameter of endoscopes is 11 mm with a 10 mm inner diameter [10]. The endoscope tip contains the tool channel, light sources, water/air outlets, and optics. These devices are located on the side on side-viewing endoscopes or duodenoscopes used in biliary examinations and operations. The duodenoscopes also have an elevator to provide additional control over the placement of the tool tip. The side of the duodenoscope contains the optics and the elevator in addition to the water/air channel. Endoscopes vary in length, diameter, number of tool channels, size of tool channels, vision system and the location of the optics. Older endoscopes used fiberoptic bundles to transmit the light to the end of the endoscope as well as viewing the tissue. The surgeon then viewed the tissue through an eyepiece at the headset. It was uncomfortable to view the tissue through the eyepiece. Large cameras where then connected to the eyepieces and the image displayed on a monitor. This arrangement was sometimes cumbersome. The large cameras were replaced with small CCD (charge coupled devices) cameras. This arrangement is called indirect video endoscopes. The CCD chips were then added to the ends of the endoscopes resulting in direct video endoscopes. The image is electronically transmitted to a video monitor. Direct endoscopes are the most popular endoscopes in modern facilities.

The endoscopic surgeon has a variety of tools to use in surgery. Four common tools used in endoscopic procedures in the colon and upper GI are shown in Figure 2. The four tools shown are the biopsy forcep, snare, cytology brush, and three-pronged grasper.

The biopsy forcep is a pair of opposing jaws which close together. The motion is controlled by the handle which slides a wire in and out of the housing. The biopsy forcep comes with or without the central prong. The central prong is a sharp piece of metal located between the two jaws. There is an electrical connection in "hot" biopsy forceps between the handle and metal jaws to provide the ability to cauterize tissue. The jaws contain teeth. The design of jaws differ in size, materials, shape of the jaws, and variations to increase the performance of the forcep to remove tissue for biopsy.

The snare is a loop of metal housed in a plastic sleeve. The metal of the snare is hardened into a loop which springs into shape once it is released from the sleeve. The in and out motion of the snare is controlled through the handle. The snare is also attached to the cautery connection in the handle.

The cytology brush is cluster of metal brushes attached to a wire surrounded by a plastic sleeve which runs back to the handle. Once again, the in and out motion of the brush is controlled by the handle.

The three-pronged grasper is similar to an "olive-plucker" and can grasp tissue and other objects. Three wires with bent tips are attached to a central wire. They spring apart when the central wire is pushed out of the sleeve and come together when the wire is pulled into

Video Controls

F

D

U

Light
Source

R

F

L

Dials

suction,
air, water
buttons

F-Fix
D-Down
U-Up
R-Right
L-Left

headset

Tool Channel

elevator

optics

side-viewing
endoscope

TOOL CHANNEL
2.8mm ID, 4 mm OD
suction, water
flash

LIGHT

LIGHT

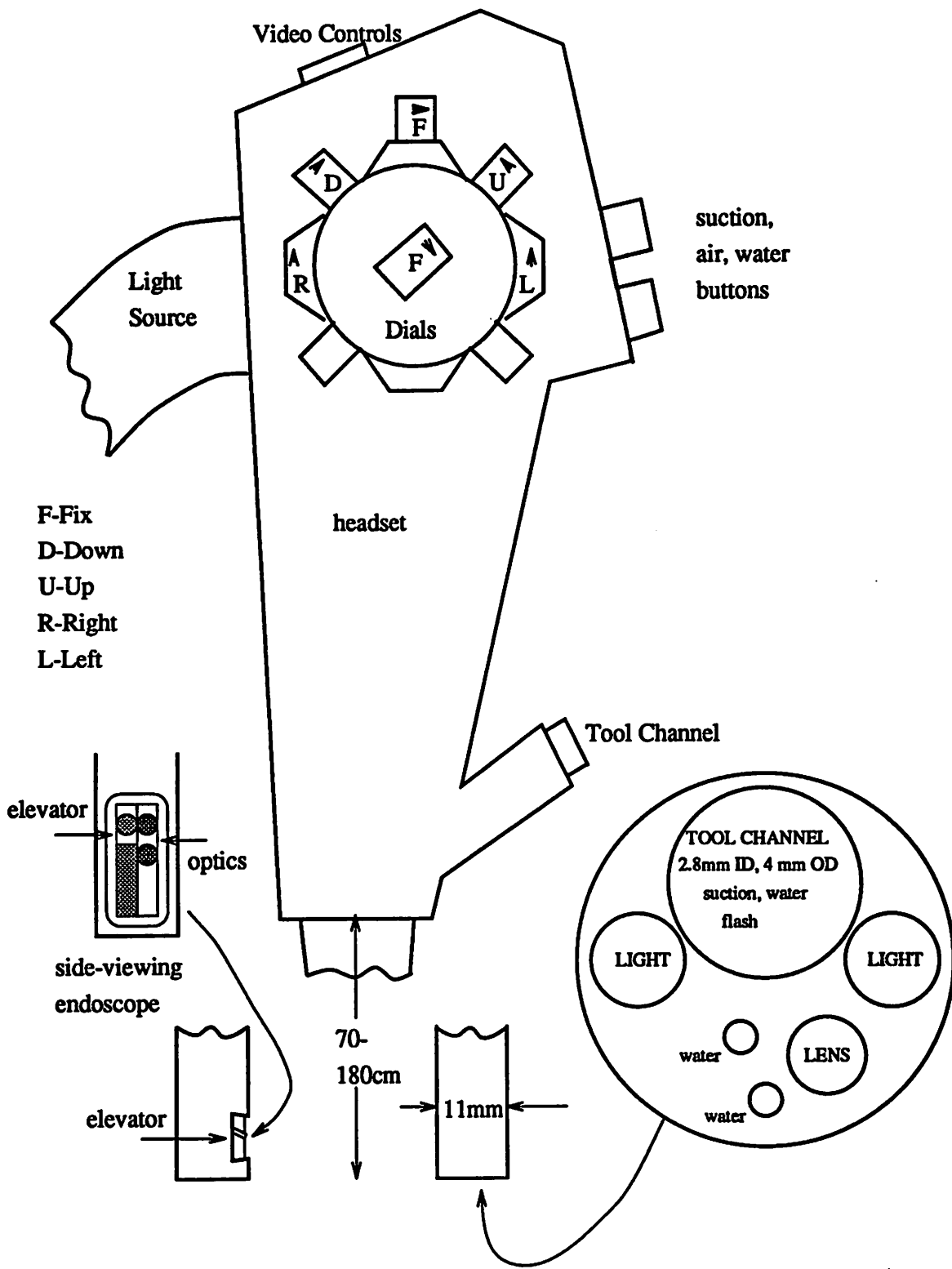LENS

water

water

70-
180cm

11mm

elevator

Figure 1: Design of Typical Flexible Endoscopes

4

the sleeve.

Four tools commonly used in endoscopic retrograde cholangiopancreatography (ERCP) are shown in Figure 3. ERCP is a technique which performs operations in the biliary tree and the pancreatic duct. These tools come in many variations including size, shape, and materials and are used in the side-viewing endoscope called a duodenoscope. These tools are used along with flouroscopy and are marked with bands which show up in the X-rays. The markings are used as a gauge of distance. Opaque to X-ray dyes are used during the procedures to view the interior of the body.

The cannula is a simple device which is built with a curvature to aid in entering a small orifice. The cannula is hollow in the middle and this is used to deliver contrast which is opaque to X-rays. The cannula has markings to gauge distance.

The papilotome or sphincterotome is a modified straight cannula used in cutting tissue. It contains a wire which when pulled, bends the plastic housing into an arch. The arch exposes the wire. The wire is connected to a power source and cuts tissue when electricity is passed through the wire. The sphincterotome is used to enlarge the openings of orifices.

The basket is a collection of 3-8 wires attached at both ends and connected to a central wire in a plastic sleeve. When the central wire is pushed out of the plastic sleeve, the wires expand and form a basket. The wires come together when the central wire is pulled into the sleeve.

The occlusion balloon is a straight cannula with a balloon attached to the end. Air pressure applied to the balloon inflates the balloon and expands as shown.

Guidewires are frequently used in ERCP. Guidewires are placed in position while other tools, such as cannulas or stents, are guided over the guidewires. The guidewires are thin and stiff wires with a typical diameter of 0.889 mm.

Biliary stents are placed into the ducts to allow drainage past blockages such as stones and tumors. They are inserted over guidewires. The guidewires are removed after the stent is in place.

3 Endoscopic Procedures

The endoscopic procedures outlined here are upper gastrointestinal (GI) endoscopy, colonoscopy, and endoscopic retrograde cholangiopancreatography (ERCP). These operations occur in the gastrointestinal tract shown in Figure 4. The upper gastrointestinal consists of the esophagus, stomach and the duodenum. Peristalsis action passes food through the esophagus, into the stomach, through the pyloric valve and into the duodenum. The liver secretes bile which flows through the common bile duct, out of the papilla of Vater and into the duodenum. Bile helps in digestion. The gallbladder stores bile secreted by the liver and also feeds into the common bile duct. Also attached to the papilla of Vater is the pancreatic duct. The pancreas secretes enzymes used in digestion which are transported through the pancreatic duct and also flow to the accessory papilla. Digestion continues through the small intestines until reaching the ileocecal valve which leads to the colon. The first part of the colon reached
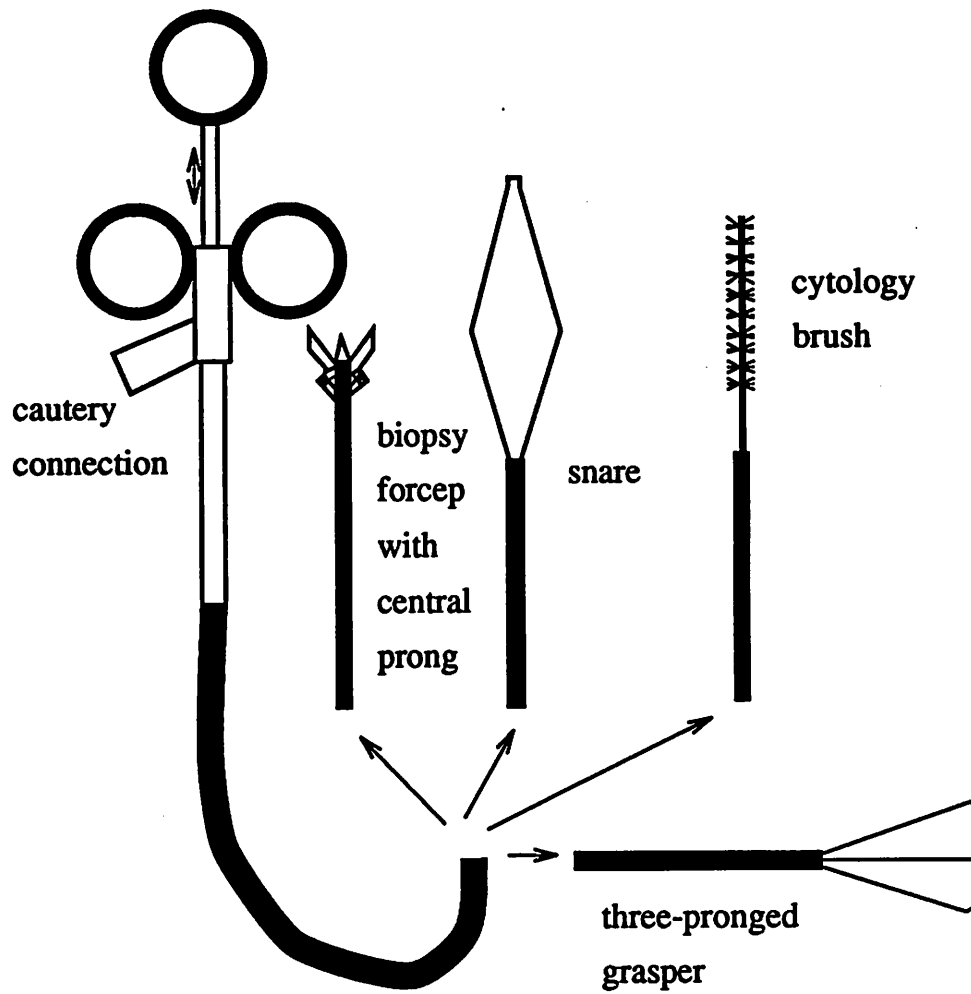
Figure 2: Common Tools used in Colonoscopy and Upper GI Endoscopy
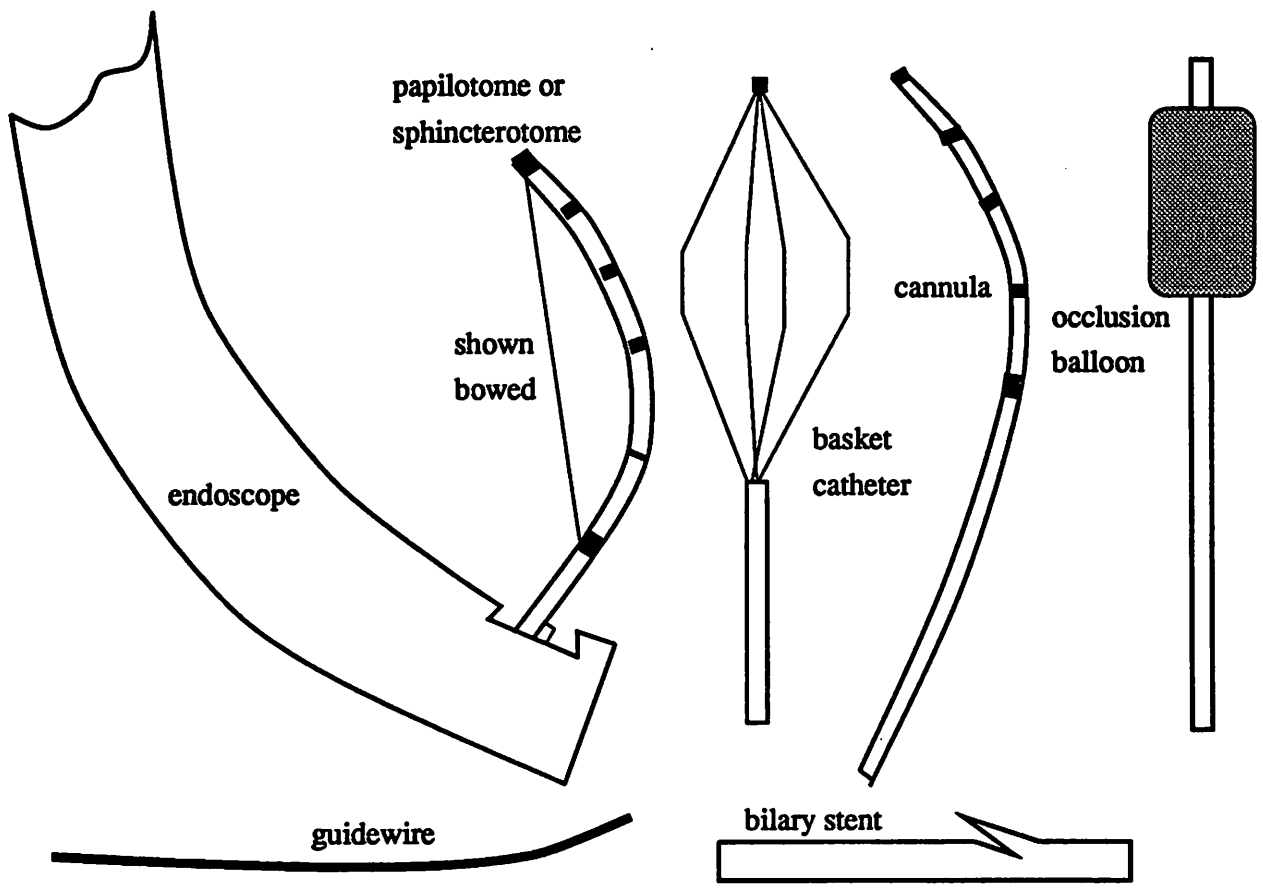
Figure 3: Common Tools used in ERCP

is the cecum which leads to the ascending colon, around the hepatic flexure, transverse colon, splenic flexure, and the descending colon. The descending colon is attached to the sigmoid colon which leads to the rectum and the anus. More information on upper GI endoscopy, colonoscopy, and ERCP is contained in [1] and [15]. A detailed atlas of the gasrointestinal tract and its diseases with video images from endoscopic procedures is contained in [16]. Much of the information provided in this section is contained in [1], [15], and [16].

3.1 Upper Gastrointestinal (GI) Endoscopy

Upper GI Endoscopy is used to examine and perform surgery in the esophagus, stomach and duodenum. This procedure is used to examine the walls of the upper GI for sources of bleeding, indications of ulcers, and look for evidence of strictures in the tract. Surgeons can then use upper GI endoscopy to treat bleeding from ulcers, tumors or vascular malformations sometimes by cauterizing the tissue with heater probes or using injections. Heater probes have rounded metal tips which are applied to the tissue as current is applied to the tip. The procedure is also used to remove swallowed or lodged foreign objects such as coins and razor blades. Snares and forceps are used to remove foreign objects. An upper GI is performed to remove polyps, place feeding tubes, install stents, take biopsies, and brush tissue for tissue samples. Polyps are removed by using snares. This procedure is described in the next subsection. Biopsies are taken with a biopsy forcep with or without a central prong. The forcep is clamped around tissue and the tissue is removed for biopsy. The biopsy sample is then taken to the lab for analysis. Some forceps allow cauterization to occur as the biopsy is taken. This fuses the tissue surrounding the biopsy sample and limits bleeding. Cauterization takes place by sending a current through the tool tip to the ground plate underneath the body. The high current density at the tip of the tool fuses the tissue. The central prong in a biopsy forcep is used to secure the forcep in tissue when the forcep is closed. This is especially helpful in the esophagus since it is difficult to hold the forcep in position since the esophagus is long, stiff, and narrow.

3.2 Colonoscopy

Colonoscopy is used to examine and perform surgeries in the colon. Colitis or inflammation of the colon walls is examined with colonoscopy. The procedure is used to determine sources of bleeding. Strictures in the colon are examined, but contrast studies are often useful. Colonoscopy is used to treat bleeding through injection or cauterization at the bleeding site, remove foreign bodies, remove polyps, dilate strictures, and biopsy tissue such as tumors and polyps.

Colonoscopy begins by preparing the colon before colonoscopy by having the patient on a no-residue diet before the procedure. This keeps the colon free of debris and makes the examination easier. The patient is sedated before the procedure to keep the patient comfortable and cooperative during the procedure. The endoscope enters the body through the anus and then into the rectum. The interior of the anus can be viewed by retroflexion,
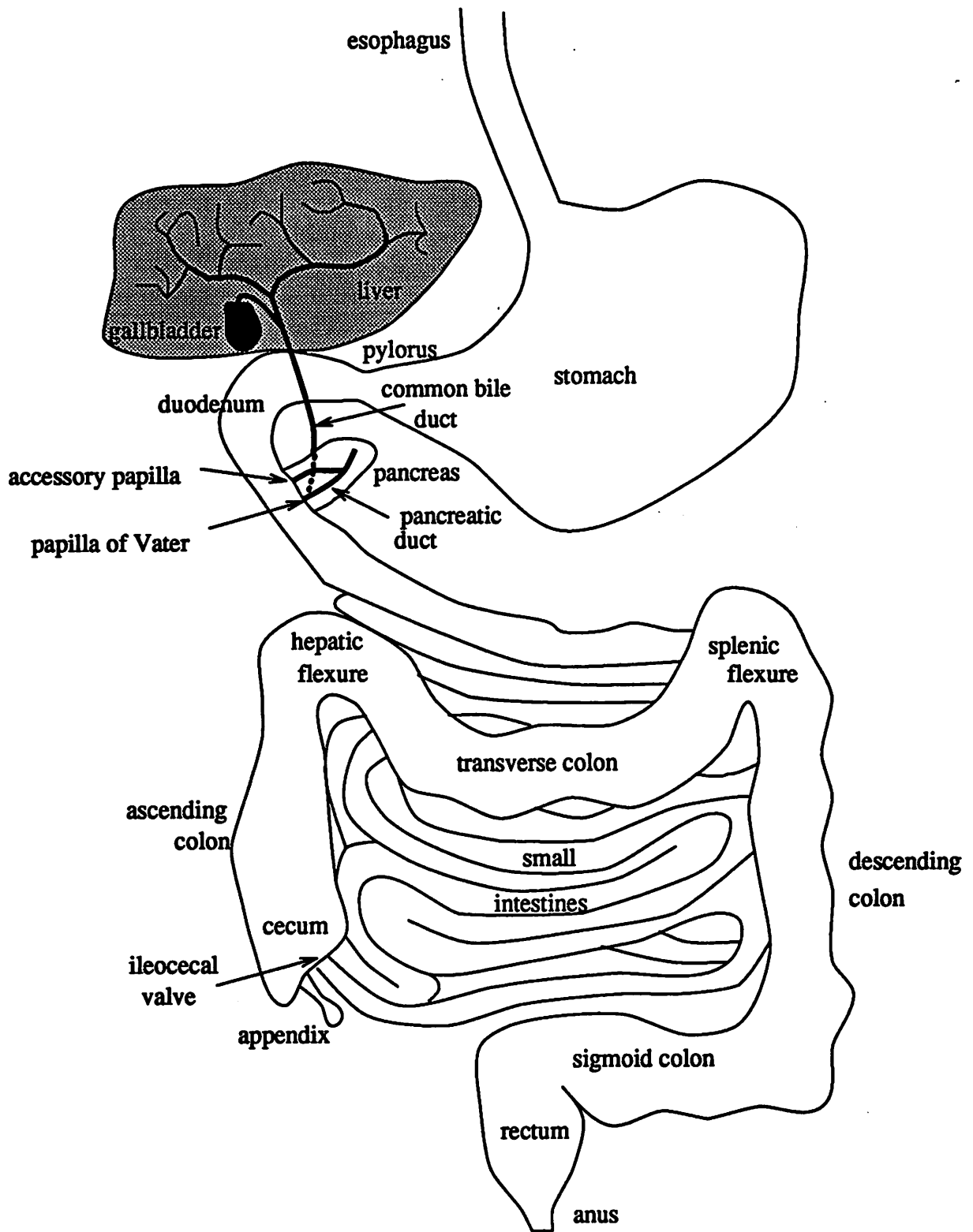
8

Figure 4: Gastrointestinal Tract

turning the endoscope onto itself, and viewing where the endoscope enters. The colon is fixed at the rectum descending colon and ascending colon. The sigmoid colon, transverse colon, and cecum are free to move on tissue called mesenteries which attach the colon to the body wall. The endoscopist uses gas to inflate the colon at times to better view the colon or help in entering the colon. Excessive amounts of insufflation make the colon rigid which hinders the passage of the endoscope. The sigmoid colon is entered after the rectum. The bends in the sigmoid colon require skill to pass the endoscope into the descending colon. The endoscope passes through the descending colon usually easily up until the splenic flexure. The endoscope makes a tight turn into the transverse colon. The transverse colon is usually passed through easily. Sometimes, the sigmoid and transverse colon can have loops which add to the difficulty in passing thought these sections. These loops also hinder progress through the rest of the colon. Passing through the hepatic flexure requires more skill than passing through the transverse colon. The endoscope then enters the ascending colon and the cecum. The ileocecal valve is then examined and can be entered to view the distal ileum. The characteristic muscular rings and folds of the parts of the colon are used as guides to the endoscopist when entering the colon. Peristaltic action is also used as a guide to the insertion of the endoscope.

Various abnormalities are viewed during colonoscopy. Colitis or inflammation of the colon is examined during colonoscopy as well as strictures although contrast studies are often more useful [1]. Diverticula, outpouches of the colon wall at sites of weakness, can be seen during colonoscopy. Polyps and tumors are examined in colonoscopy. Colonic polyps vary in shape and size. Pendunculated polyps are mushroom shaped polyps which have rounded heads attached to a stalk which secures the polyp to the colon wall. Sessile polyps do not have a stalk and are not raised up on a stalk.

One use of colonoscopy is the removal and biopsy of polyps and tumors. Biopsies are performed in the same way as in upper GI endoscopy, however, the biopsy forcep usually travels much farther in colonoscopy. A biopsy forcep which is attached to a electrocautery machine is used to remove small polyps. The forcep surrounds the head of the polyp. The stalk is cauterized but the tissue in the interior of the forcep is not damaged and is examined for biopsy.

Polypectomy is the removal of polyps from the colon. It can sometimes be very difficult and require skill. The snare is slipped over the head of a pedunculated polyp. The snare is tightened by pulling the snare into the plastic sheath while the sheath is positioned at the base of the polyp. See Figure 5. A pseudostalk can be created in a sessile polyp by grabbing the surrounding tissue of the polyp and tightening the snare. The handle of the snare is tightened but not overtightened. The head of the polyp is then lifted off of the wall to increase the current density at the tool tip. The snare is then tightened further as coagulation current is applied to cauterize the tissue and lessen bleeding. Sometimes there are blood vessels in the interior of the stalk of the polyp. A larger stalk is more likely to contain a blood vessel than a smaller stalk [1]. The snare surrounds the vessel with pressure and cuts off blood flow as it is cauterized. The coagulation current may be varied as the
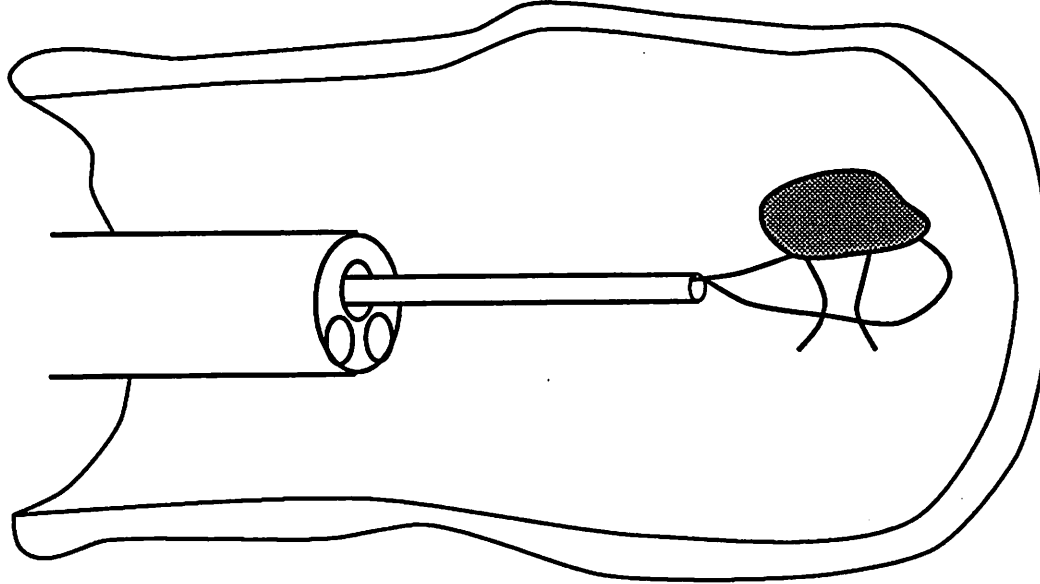
Figure 5: Polyp Removal

snare is tightened. After the polyp is removed, it can be sucked into the suction trap or picked up later with a three-pronged grasper. Some endoscopists suck the polyp as it is removed which saves time retrieving the polyp [14]. The polyp and biopsies are sent to the lab for examination.

3.3 Endoscopic Retrograde Cholangiopancreatography (ERCP).

ERCP is a technique used to opacify the biliary tree and pancreatic duct system in the duodenum and perform endoscopic surgeries in this area. The procedure is performed on patients who are experiencing jaundice or are suspected of pancreatic or biliary tract disease. It is used to examine narrowing or strictures in the colon bile and pancreatic ducts and in the orifices, such as the papilla of Vater. Sphincterotomy of the duodenum papilla is performed during ERCP. Common bile stones are removed through this procedure. Stents are placed in the common bile duct (CBD) and the pancreatic duct (PD) to allow bile and the enzymatic juices to flow past strictures caused by tumors and unremovable stones. Balloon dilation of strictures is performed to open up the duct and resume the flow. Nasobiliary drains are placed into the CBD to allow drainage of bile through a tube placed in the nose, through the esophagus and into the CBD. Tubes are also placed into the ducts to allow infusion of chemicals to dissolve and flush out stones.

The side-viewing endoscope or duodenoscope is sent down through the throat, esophagus, stomach and into the duodenum. The side of the instrument with the video and elevator is placed to face the papilla of Vater. The papilla of Vater is a small orifice and takes skill to locate. It is seen to normally be a small bud on the wall which contains a orifice.

Once the duodenoscope is in position, a cannula can be used to enter the CBD or the PD. The CBD is entered with the cannula entering from below the papilla (below refers to being further down the duodenum). The cannula usually has a curve to aid in entering the CBD. The PD is entered by angling the cannula downward. The cannula is pushed further into one of the ducts. Contrast, which is opaque to X-ray, is then injected into the duct. The image on the flouroscopy monitor reveals strictures, stones, and the condition of the ducts. The proper dilution of contrast is necessary so that stones show up in the X-ray. The X-ray is not on continuously but activated for seconds at a time to view the status of the procedure. The cannula has markings which show up on X-ray. These markings give a gauge of the depth of penetration.

The papillotome is used to increase the diameter of the CBD opening to allow easier access to the duct and to allow easier removal of stones. The papillotome is inserted into the orifice and tension is applied to the cutting wire. Current is passed thought the cutting wire as tension is applied to cauterize the tissue as it is cut. Tension in the papillotome cutting wire causes the papillotome to curve. The papillotome is sometimes used instead of the cannula to enter and opacify the duct.

The retrieval basket is used to remove CBD stones out of the papillotomed orifice. See Figure 6. The basket is inserted into the orifice and is positioned around a stone. The most distal stone is removed first as shown in Figure 6 (distal is in relation to the direction of the flow of fluid). The wire basket surrounds the stone and is captured when tension is applied to the stone. The stone is then removed and dropped into duodenum. There is a special tool which attaches to the handle of a strong basket which provides adequate pressure to crush the stones or break the basket. This is useful when the stone and basket become lodged in the duct perhaps from trying to grab too may stones at once.

Occlusion balloons have various uses. One use is to block the duct so that contrast can be injected under pressure and through strictures. The surgeon needs to be careful when injecting contrast through strictures since the contrast needs to be removed or allowed to drain out. Otherwise, the patient may experience a bacterial infection. The balloon is used to remove stones as well. The deflated balloon is passed past the stones, inflated, and pulled out into the duodenum. This can remove stones from the duct. A third use is to open up strictures by inserting the deflated balloon into a stricture and inflating the balloon.

Guidewires are placed inside the duct and other tools such as cannulas or stents are guided over the wire. It is sometimes easier to first insert the guidewire and then insert the stent rather than inserting the stent alone. Caution must be used so that the duct is not perforated.

Stents are tubes which are inserted into the duct to allow drainage past obstructions. The stents have flaps which help to hold the stent in place once inserted into the duct. Stents are removed once they become blocked. The stents are removed by grabbing onto the stent with a snare or retrieval basket and pulling it into the duodenoscope.

Nasobiliary drains are also installed through ERCP. These allow drainage of bile through a tube from the CBD out through the nose. The drainage tubes have flaps which hold the

common
bile
duct

gallstones

duodenoscope

basket

pancreatic
duct
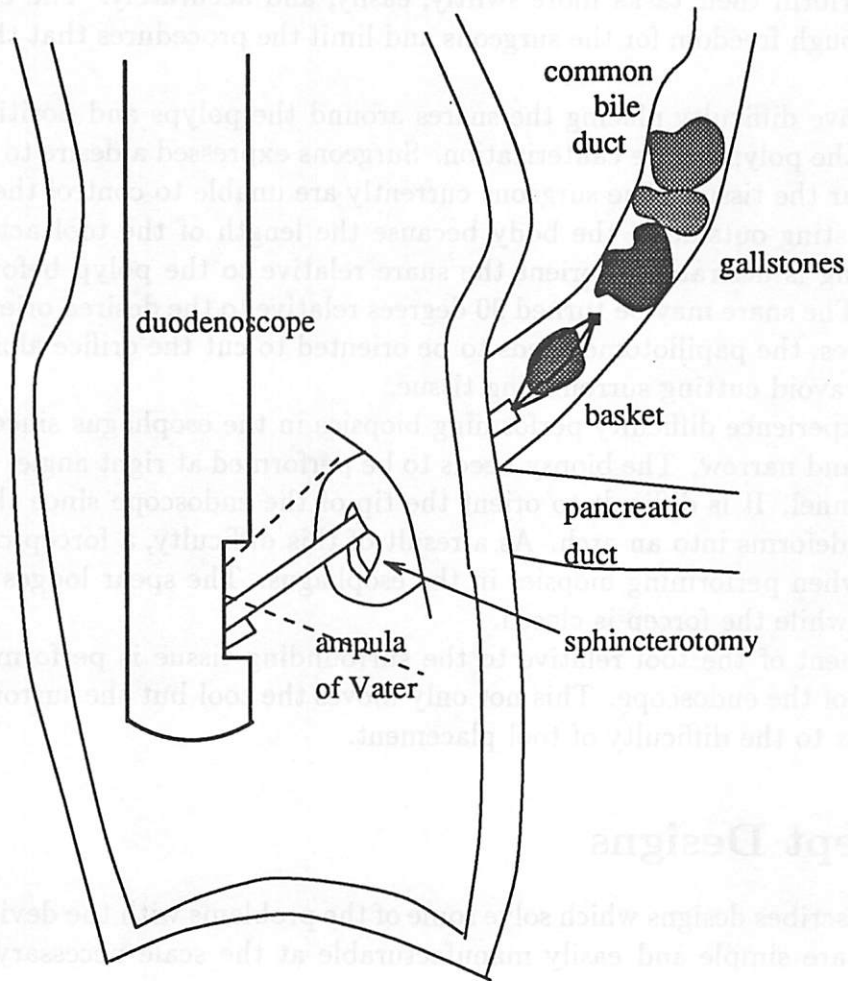
sphincterotomy

ampula
of Vater

Figure 6: CBD Stone Removal

tube in place in the CBD. Chemicals are sometimes flushed through these tubes to dissolve stones. Saline solutions are also flushed to dislodge stones and stone fragments.

4   Limitations of Current Instruments

There is a need for better tools and equipment to give surgeons more flexibility and allow the surgeons to perform their tasks more swiftly, easily, and accurately. The existing tools do not provide enough freedom for the surgeons and limit the procedures that they can perform endoscopically.

Surgeons have difficulty placing the snares around the polyps and positioning the snare on the base of the polyp before cauterization. Surgeons expressed a desire to be able to twist the tool tip near the tissue. The surgeons currently are unable to control the twisting of the tool tip by twisting outside of the body because the length of the tool acts as a torsional spring. Twisting is desirable to orient the snare relative to the polyp before performing a polypectomy. The snare may be turned 90 degrees relative to the desired orientation. During sphincterotomies, the papillotome needs to be oriented to cut the orifice along the direction of the CBD to avoid cutting surrounding tissue.

Surgeons experience difficulty performing biopsies in the esophagus since this channel is straight, rigid and narrow. The biopsy needs to be performed at right angles to the direction of the tool channel. It is difficult to orient the tip of the endoscope since the last 10 cm of the endoscope deforms into an arch. As a result of this difficulty, a forcep combined with a spear is used when performing biopsies in the esophagus. The spear lodges into the side of the esophagus while the forcep is closed.

The placement of the tool relative to the surrounding tissue is performed by orienting the last 10 cm of the endoscope. This not only moves the tool but the surrounding tissue as well which adds to the difficulty of tool placement.

5   Concept Designs

This section describes designs which solve some of the problems with the devices listed above. These designs are simple and easily manufacturable at the scale necessary for endoscopic surgery.

5.1   Snare-Forcep Combination

A new tool is created by combining the snare with the forcep. This tool makes it easier to snare polyps. Once the polyp is secured with the forcep, the snare slips over the forcep and around the polyp. The polyp is removed and the forcep can carry the polyp into the suction channel to be removed. This simple tool will make it easier to snare polyps since it is easier to grab the polyp with the forcep than with the snare and makes removing the
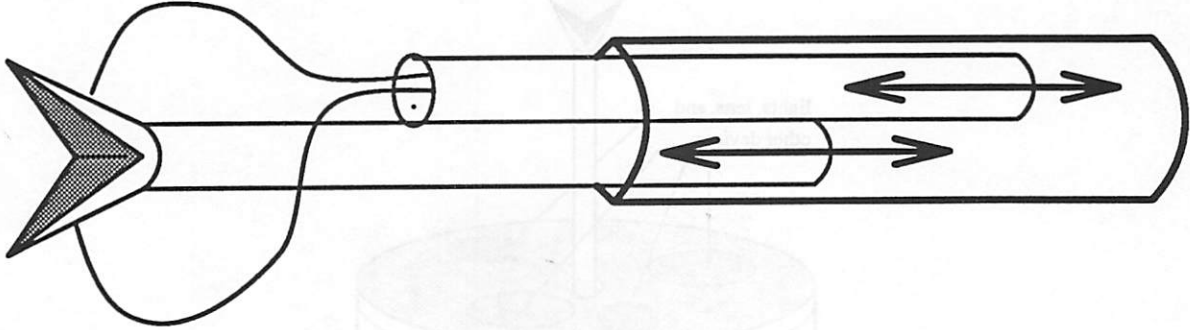
Figure 7: Snare and Forcep Combination

polyp easier because the polyp does not have to be recovered after it is severed. It will allow
more accuracy in the location of the cut. The tool is shown in Figure 7. A key point is that
the snare needs to surround the forcep before the forcep secures the polyp. The snare and
forcep may need to be placed in the original position if a grasp is unsuccessful. This can be
designed into the device by not letting the snare rotate relative to the forcep and by placing
a permanent bend in the snare which orients the snare so that the forcep always points into
the snare opening. The snare and forcep move in and out independently. The concept for
this design came out of discussions with Curt Deno, Brad Smallridge, and the author of this
report.

5.2 Endo-Platform

Manipulating the placement of the tool in current endoscopes is done by sliding the tool
in and out of the channel and by deforming the last 10 cm of the endoscope into an arch.
Changing the position of the patient and pushing on the patients abdomen is another way of
changing the position of the tool relative to the tissue. The surgeon must move the entire 10
cm of the end of the endoscope to slightly reposition the tool. This moves the surrounding
tissue and adds difficulty positioning the tool at the desired configuration. A device which
allows a surgeon to reorient the tool without moving the surrounding tissue would allow the
surgeon to more accurately and swiftly position the tool. Reorienting the tool and not the
lens would not be as beneficial as moving the lens along with the tool because the tool tip
quickly goes out of view of the video. The endo-platform provides this additional freedom
in placing the tool. This device is shown in Figure 8. It is composed of two plates separated
by rigid tubes and a short spring. The diameter of the plates is the same as the diameter of
the endoscope. The spring serves as a spherical joint. The spherical joint resists side forces
and provides a pivot point. By individually pulling on the tendons, the outer plate changes
orientation relative to the inner plate. It was recently noticed that the original design to
orient the outer plate relative to the inner plate from which the current design was developed
is similar to a design seen in [8]. The tool slides through both plates and the same devices on
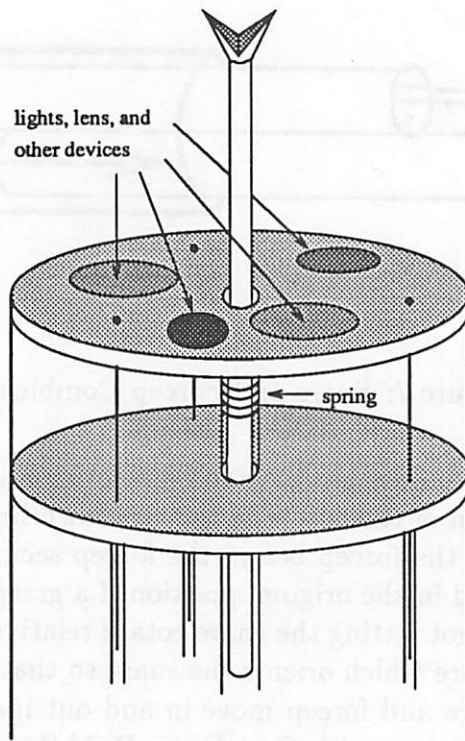the tip of a normal endoscope are on the outer plate. The position of the tool tip is changed

Figure 8: Endo-Platform

by pulling on the tendons. The viewing area of the lens moves with the tool as well as the CCD array. The water channels are flexible between the two plates to accommodate the motion. The endo platform is attached to the end of an existing endoscope. Large motions are controlled by deforming the last 10cm into an arch. Fine motions are accomplished by fixing the arch and reorienting the outer plate relative to the inner plate of the endo-platform. Fine motions would be controlled by a joystick located where the tool is currently inserted into the endoscope headset. The tendons are then actuated by an array of DC motors. In this way, the surgeon can control the in and out motion of the tool as well as the orientation of the tool.

5.3 Rotary Actuators

The addition of rotary motion would help the surgeons accurately position the tools onto or into the tissue. Designing a rotary actuator to fit into the tip of the endoscope is a difficult task. It is difficult to provide rotary motion when there is little space perpendicular to the axis of revolution. Three rotary actuator designs are described in this subsection.

The first design uses a high pitch screw in a fixed housing attached to a small piston, such as the pistons described in [2]. The design is shown in Figure 9. As the screw is pushed or pulled through the housing, the screw rotates. Tendons can also be used to push and to
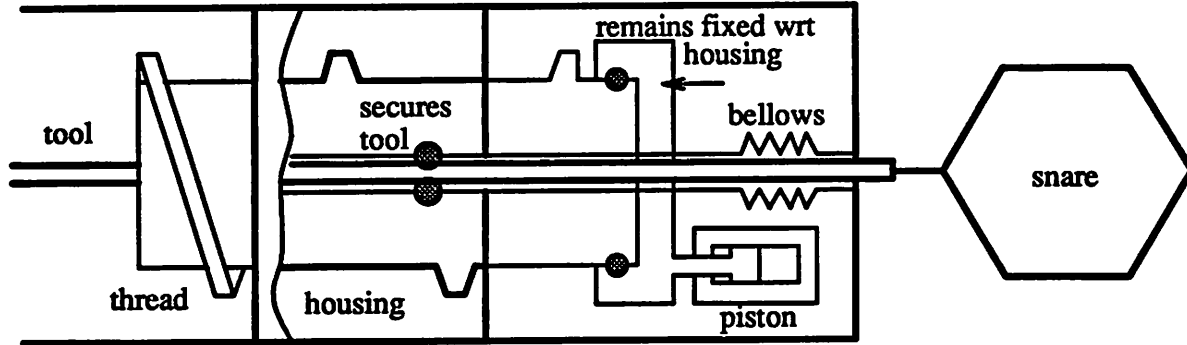
Figure 9: Rotary Screw Actuator

pull on the screw. The tool would be secured to the interior of the screw and would rotate as the screw rotates. The housing of the tool needs to be secured to the part of the tool which operates on the tissue. For example, in current snares, the housing of the tool is a plastic tube and the metal wire is what operates on the tissue. The wire and the tube are not fixed but can be made to be rotationally fixed through design modifications.

The second design is composed of a central pulley and two smaller pulleys. This actuator is driven by tendons. As the tendons are pulled, the central pulley spins in the fixed housing. The tool is fixed to the central pulley and rotates as the tendons are pulled. The design is shown in Figure 10.

The third design uses a flexible shaft to transmit linear motion about an axis to rotation about the same axis. The design is shown in Figure 11. There is a central tool chuck which holds the tool and spins. In the center of the tool channel is an O-ring which secures the tool. Next to the tool chuck is a cylinder which spins the tool chuck. This cylinder is attached to a flexible shaft which is attached to a pulley. Tendons attached to the pulley spin the pulley which spins the shaft which finally spins the tool.

A comparison of these designs reveals that each has advantages and disadvantages over the other. The screw actuator is pushed and pulled off center since the tool needs to run through the center of the screw. This may result in the screw actuator jamming. The screw, by design, moves along the axis of rotation as the screw rotates while the central pulley remains fixed in the pulley design as the tool is rotated. The two smaller pulleys require additional space out of the cross section of the endoscope while the piston only requires one area of the cross section. The flexible shaft design requires additional area in the cross section.

5.4   Combining the Tools

The tools described in the previous subsections can be combined into a single tool. The rotary actuator can be combined with the endo-platform to provide additional dexterity to the endoscopic surgeon. The snare-forcep tool can be used together with the rotary-endo-platform to provide more freedom.
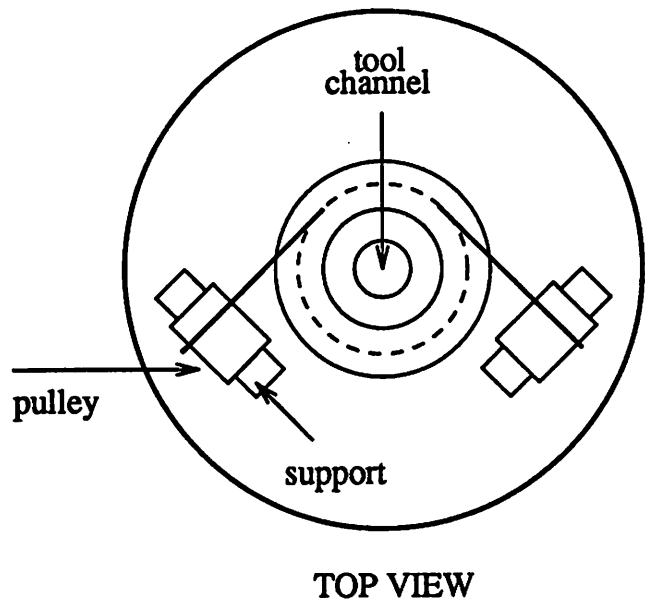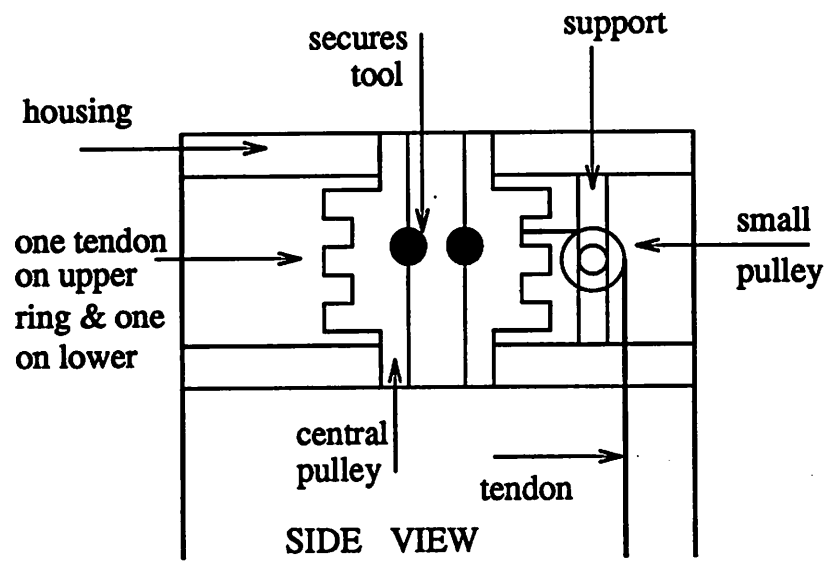
17

secures
tool

support

housing

one tendon
on upper
ring & one
on lower

small
pulley

central
pulley

tendon

SIDE VIEW

tool
channel

pulley

support

TOP VIEW

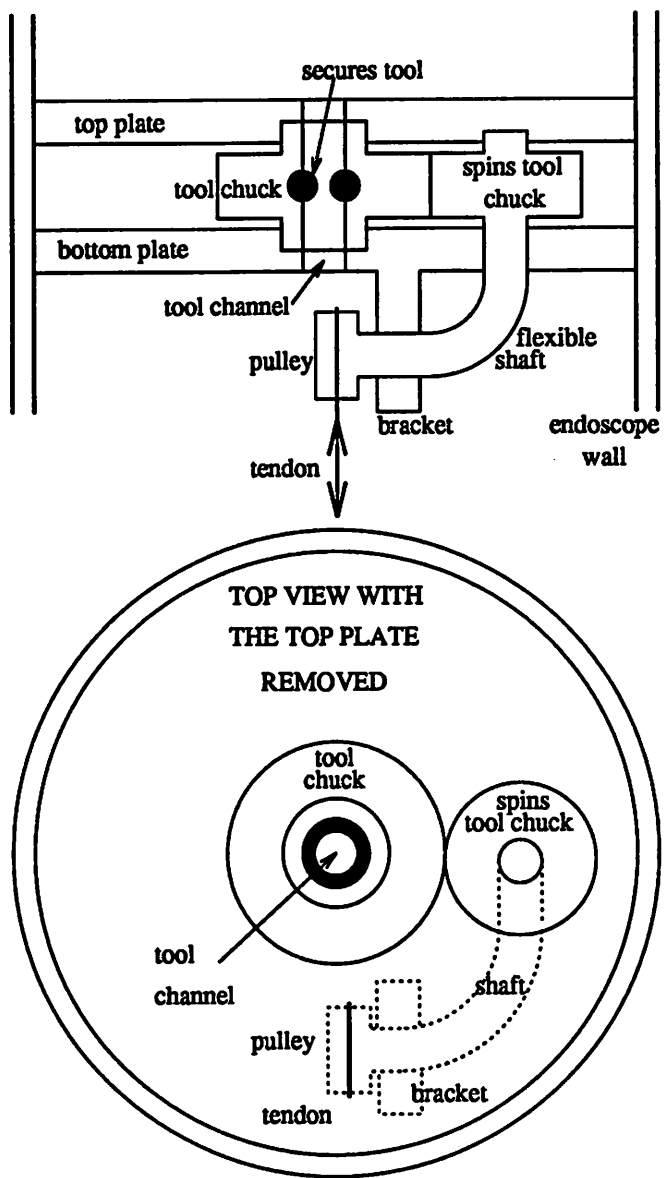Figure 10: Rotary Pulley Actuator

18

Figure 11: Flexible Rotary-Shaft Actuator

6 Detailed Design of the Endo-Platform

The endo-platform is described in more detail in this section. The goals of the design are presented, and it is shown how the platform meets these goals. The kinematic model is presented along with the kinematic analysis. The dynamic equations are developed and presented. Using the kinematic model and the dynamic model, a control algorithm is presented and described. The dynamic equations with the controller are simulated. A step to the desired tool position is commanded and the resulting trajectory is shown. A brief description of the prototype device is shown to conclude the section.

6.1 Design Goals

This section presents the design goals for the endo-platform. The goals evolved as the designed evolved and our experience with the problem increased. The endo-platform will be incorporated into the endoscope or will become a disposable attachment to endoscopes which can accept it. The device should be compatible with existing endoscopic equipment and work with current tools with minimal modifications. Redesign of existing equipment should be minimized to decrease the time to manufacture. The device is designed to give the surgeon more dexterity than current instruments. The design should be kept as simple as possible and facilitate manufacture at the small scales. Cost is a concern in the design. This concern becomes more important if the device is to be disposable. The design should use existing technology with demonstrated reliability as much as possible. The endo-platform's main goal is to provide fine adjustments to the endoscopic surgeon. The harsh environment experienced by the tool requires the tool to be rugged. If the tool is permanently attached to an endoscope tip, then the tool must withstand the sterilization process. This enforces additional requirements on the materials used. The control of the device is a concern in the design of the mechanical function of the tool. The tool is designed to facilitate control design. The control design and tool design proceeds in a *concurrent design methodology*. The device should have an intuitive user interface. The design should allow a natural mapping between tool movement and surgeon input.

6.2 Kinematic Model and Analysis

The kinematic model of the device is shown in Figure 12. The following development describes the figure. In this model, the top plate and the bottom plate are connected through a spherical joint. The three lines in the top plate which radiate from a central point connect the tool axis to the points where the tendons are attached. Similarly, the bottom plate has three radial lines attaching the bottom tool axis to the locations where the tendons pass through the bottom plate. The length of the radial lines is rt for the top plate and rb for the bottom plate. The distance from the bottom plate to the pivot point is d, and the distance from the top plate to the pivot point is dt. These four parameters characterize the particular geometry of the manipulator. The tendons are fixed to the top plate but slide through the
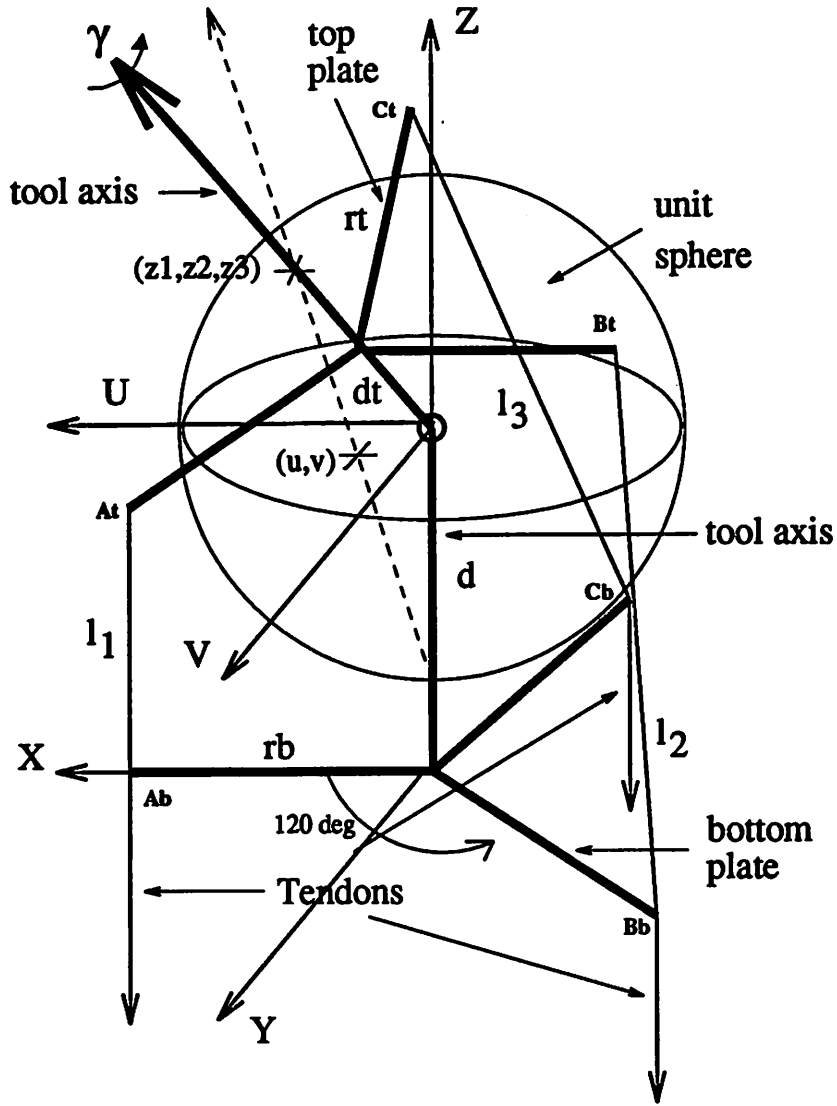
Kinematic Model

Figure 12: Kinematic Model

points in the bottom plate. The tendon lengths between the top and bottom plates are l_1, l_2, and l_3. The tool axis runs through the center of both plates. The radial lines are equally spaced 120 degrees apart and lie in the plane formed by the three points where the tendons are attached. The tendons are fixed to the top plate and are strung through the bottom plate. The orientation of the top plate is controlled by pulling on the tendons. The pointing direction is controlled by controlling the orientation of the top plate since the tool points in a direction normal to the surface of the top plate.

The tool position is given by three coordinates, (u, v, γ). The three coordinates are grouped into the vector, θ. There are three frames which are important in the kinematic model and which are used in the dynamic analysis which follows. There are two spatial frames and one body frame. The spatial frames are fixed in inertial space and the body frame is fixed to the moving top plate. The XYZ frame is a spatial frame. The XY plane lies in the bottom plate and the origin is the intersection of the tool axis with the bottom plate. The X axis is aligned with the line from the origin to the point labeled Ab. The Y axis is 90 degrees to the X axis and is defined such that the right hand frame defines a Z axis pointing upwards through the tool axis. The second spatial frame, the UVZ frame, is attached to the pivot point and the axes are parallel to the XYZ axis. Translating along the tool axis fixed to the bottom plate by the vector $(0, 0, d)$ brings the UVZ frame coincident with the XYZ frame. The body frame (not shown in the figure) is attached to the top plate and is initially coincident with the UVZ axis when in the home configuration. The home configuration occurs when the tool axis in the top plate is parallel to the tool axis in the bottom plate and when the tendon attachment points in both plates are vertically aligned. The home configuration is denoted, $(u, v, \gamma) = (0, 0, 0)$. For our dynamic model, the spherical bearing consists of a spring which can bend laterally and also twist. The γ coordinate corresponds to the amount of twist in the spring about the longitudinal axis of the spring. The longitudinal axis is aligned with the tool axis in both the top plate and the bottom plate at the point of attachment. Pure bending or no twist of the spring occurs when $\gamma = 0$. Pure bending is a rotation of the body frame by an axis lying in the UV plane. Any body frame orientation can be obtained by a pure bending rotation followed by a twist rotation. The twist rotation is a rotation about the body frame Z axis. Given an arbitrary body frame orientation, perform a pure bending rotation to align the Z axis of the desired frame orientation and the frame obtained through pure bending. Then perform a twist about the current body Z axis to align the remaining axes. The u and v coordinates parameterize the no bending rotation. This parameterization has a singularity when the tool points directly downward. The (u, v) coordinates are obtained as follows: First, form a unit sphere in the length unit chosen. For this analysis, the length unit of a centimeter was chosen. The tool axis in the top plate intersects the unit sphere. Draw a line from the south pole, $(0, 0, -1)$ in the UVZ frame, through the point of intersection of the tool axis with the sphere, see Figure 12. This line intersects the UV plane at a point. This point is the (u, v) coordinate. This choice of coordinates is a modified stereographic projection. These seemingly unintuitive coordinates where chosen to avoid singularities in the parameterization

in the expected tool configurations and to lead to tractable dynamic equations. These set of coordinates lead to a simple form for the dynamic equations which are described in the next section. Similar choice of coordinates are used in modeling of the eye where one wants to minimize the twisting in the optic nerve [5]. In this case, the spherical spring joint is identified with the optic nerve. In the analysis of the reorientation of the falling cat, similar coordinates have been used to model the joint in the spinal column of true cats [18].

The rotation matrix which represents the top plate orientation with respect to the UVZ plane is now described. The map from coordinates in the unit sphere to coordinates in the UV plane is

$$(u, v) = \frac{1}{1 + z_3} (z_1, z_2).$$ (1)

The coordinates in the unit sphere are (z_1, z_2, z_3). This result follows easily from similar triangles. Notice that the map is not defined when $z_3 = -1$. The inverse map is given by

$$(z_1, z_2, z_3) = (ut, vt, t - 1)$$ (2)

where $t = \frac{2}{1+u^2+v^2}$. As stated in [7], the rotation matrix formed by rotating about an axis $k = (k_x, k_y, k_z)^T$ by an angle ϕ is given by

$$Rot\,(k, \phi) = \begin{bmatrix} k_x k_x v_\phi + c_\phi & k_y k_x v_\phi - k_z s_\phi & k_z k_x v_\phi + k_y s_\phi \\ k_x k_y v_\phi + k_z s_\phi & k_y k_y v_\phi + c_\phi & k_z k_y v_\phi - k_x s_\phi \\ k_x k_z v_\phi - k_y s_\phi & k_y k_z v_\phi + k_x s_\phi & k_z k_z v_\phi + c_\phi \end{bmatrix},$$ (3)

where $c_\phi = cos(\phi)$, $s_\phi = sin(\phi)$, and $v_\phi = 1 - c_\phi$. The no twist rotation which rotates the tool axis from the vertical direction corresponds to a rotation about a unit vector lying in the UV plane. This vector is the normalized vector resulting from the cross product between the vertical axis and the current body tool axis. The axis of rotation is then

$$k = \frac{1}{\sqrt{z_1^2 + z_2^2}} \begin{bmatrix} -z_2 \\ z_1 \\ 0 \end{bmatrix}.$$ (4)

The angle of rotation is the angle the current body axis makes with the vertical axis (see Figure 13). Using the relationships,

$$\begin{aligned} c_\phi &= z_3 \\ s_\phi &= \sqrt{z_1^2 + z_2^2} \\ v_\phi &= 1 - z_3, \end{aligned}$$ (5)

and (4) and substituting into (3) yields the no-twist rotation matrix in terms of the coordinates in the sphere,

$$R_{nt}\,(z_1, z_2, z_3) = \begin{bmatrix} \frac{z_2^2}{1+z_3} + z_3 & \frac{-z_1 z_2}{1+z_3} & z_1 \\ \frac{-z_1 z_2}{1+z_3} & \frac{z_1^2}{1+z_3} + z_3 & z_2 \\ -z_1 & -z_2 & z_3 \end{bmatrix}.$$ (6)
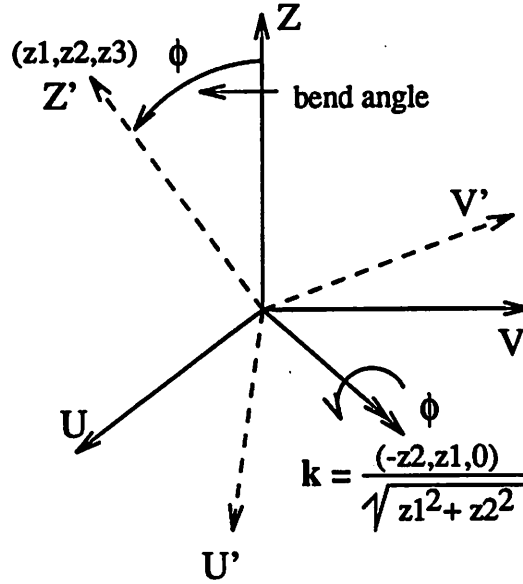
Figure 13: No Twist Rotation

Using (2) and substituting into (6) gives

$$R_{nt}(u,v) = \frac{t}{2} \begin{bmatrix} 1 - u^2 + v^2 & -2uv & 2u \\ -2uv & 1 + u^2 - v^2 & 2v \\ -2u & -2v & 1 - u^2 - v^2 \end{bmatrix}. \tag{7}$$

The rotation matrix which maps points in the body frame to points in the spatial UVZ frame is $R(u,v,\gamma) = R_{nt}(u,v) R_z(\gamma)$, where

$$R_z(\gamma) = \begin{bmatrix} c_\gamma & -s_\gamma & 0 \\ s_\gamma & c_\gamma & 0 \\ 0 & 0 & 1 \end{bmatrix}. \tag{8}$$

The tendon lengths between the top and bottom plates are calculated as follows: The distance is calculated between the points A_b and A_t, B_b and B_t, and C_b and C_t defined in Figure 12. The position of the points in the top frame with respect to the UVZ frame is obtained by mapping the points through the rotation matrix. The coordinates of the points are easily determined in the XYZ spatial frame. The distances are then calculated by determining the magnitude of the vector joining the two points in the XYZ frame. This procedure defines a map from (u,v,γ) to (l_1, l_2, l_3) space. The tendon lengths parameterized by u and v ranging between -0.7 to 0.7 with $\gamma = 0$ is shown in Figure 14. This function and its differential are contained in the Appendix. Assuming that $\gamma = 0$ for all time results in a jacobian which is a 3 × 2 matrix. The null space of the transpose of this jacobian is the normal to the surface shown in Figure 14.

24

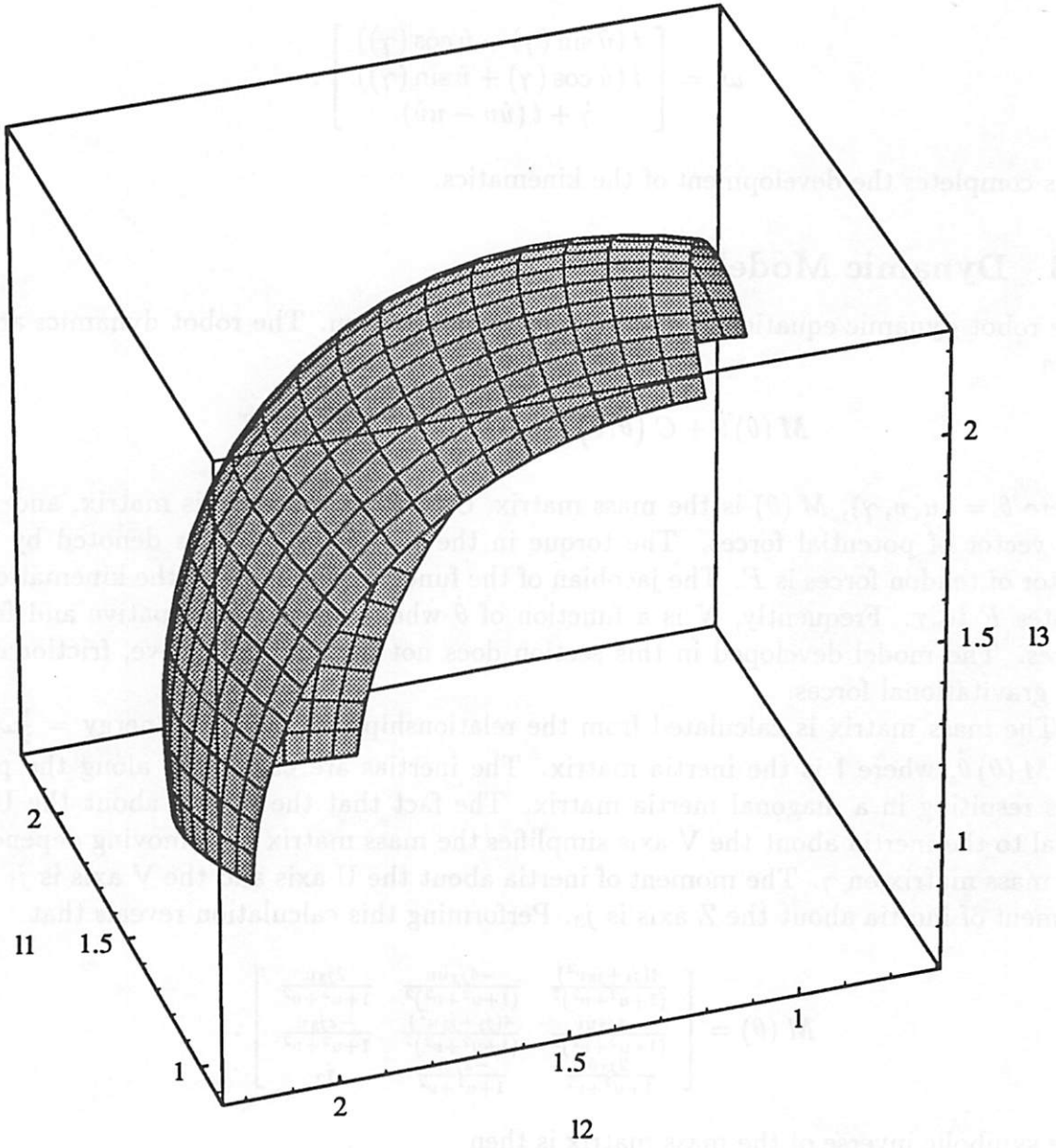Tendon Lengths Parameterized by u and v

Figure 14: Parameterized Tendon Lengths

The body angular velocity is needed for the determination of the kinetic energy used in calculating the dynamic equations. The body angular velocity, ω_b, written as a skew-symmetric matrix is $\hat{\omega}_b = R^T \dot{R}$. See [12] for more details on this description of the body angular velocity. Carrying out the calculations in Mathematica [19] results in the following expression:

$$\omega_b = \begin{bmatrix} t\left(\dot{u}\sin\left(\gamma\right) - \dot{v}\cos\left(\gamma\right)\right) \\ t\left(\dot{u}\cos\left(\gamma\right) + \dot{v}\sin\left(\gamma\right)\right) \\ \dot{\gamma} + t\left(\dot{u}v - u\dot{v}\right) \end{bmatrix}. \tag{9}$$

This completes the development of the kinematics.

6.3 Dynamic Model

The robot dynamic equations are developed in this section. The robot dynamics are of the form

$$M\left(\theta\right)\ddot{\theta} + C\left(\dot{\theta},\theta\right)\dot{\theta} + N\left(\theta\right) = \tau = J^T\left(\theta\right)F \tag{10}$$

where $\theta = (u,v,\gamma)$, $M\left(\theta\right)$ is the mass matrix, $C\left(\dot{\theta},\theta\right)$ is the coriolis matrix, and $N\left(\theta\right)$ is the vector of potential forces. The torque in the tool coordinates is denoted by τ. The vector of tendon forces is F. The jacobian of the function discussed in the kinematic section relates F to τ. Frequently, N is a function of $\dot{\theta}$ when there are dissipative and frictional forces. The model developed in this section does not include dissipative, frictional forces, nor gravitational forces.

The mass matrix is calculated from the relationship that Kinetic Energy $= \frac{1}{2}\omega_b^T I \omega_b = \frac{1}{2}\dot{\theta}^T M\left(\theta\right)\dot{\theta}$, where I is the inertia matrix. The inertias are calculated along the principal axes resulting in a diagonal inertia matrix. The fact that the inertia about the U axis is equal to the inertia about the V axis simplifies the mass matrix by removing dependence of the mass matrix on γ. The moment of inertia about the U axis and the V axis is j_1 and the moment of inertia about the Z axis is j_3. Performing this calculation reveals that

$$M\left(\theta\right) = \begin{bmatrix} \frac{4(j_1+j_3 v^2)}{(1+u^2+v^2)^2} & \frac{-4j_3 uv}{(1+u^2+v^2)^2} & \frac{2j_3 v}{1+u^2+v^2} \\ \frac{-4j_3 uv}{(1+u^2+v^2)^2} & \frac{4(j_1+j_3 u^2)}{(1+u^2+v^2)^2} & \frac{-2j_3 u}{1+u^2+v^2} \\ \frac{2j_3 v}{1+u^2+v^2} & \frac{-2j_3 u}{1+u^2+v^2} & j_3 \end{bmatrix}. \tag{11}$$

The symbolic inverse of the mass matrix is then

$$M^{-1}\left(\theta\right) = \begin{bmatrix} \frac{(1+u^2+v^2)^2}{4j_1} & 0 & \frac{-v(1+u^2+v^2)}{2j_1} \\ 0 & \frac{(1+u^2+v^2)^2}{4j_1} & \frac{u(1+u^2+v^2)}{2j_1} \\ \frac{-v(1+u^2+v^2)}{2j_1} & \frac{u(1+u^2+v^2)}{2j_1} & \frac{1}{j_3}+\frac{u^2+v^2}{j_1} \end{bmatrix}. \tag{12}$$

26

The Coriolis matrix is derived from the mass matrix by the following formula for the ijth element. See [12] for a derivation.

$$C_{ij}\left(\dot{\theta},\theta\right) = \frac{1}{2}\sum_{k=1}^{n}\left(\frac{\partial M_{ij}}{\partial\theta_k} + \frac{\partial M_{ik}}{\partial\theta_j} - \frac{\partial M_{jk}}{\partial\theta_i}\right)\dot{\theta}_k. \tag{13}$$

Performing these calculations and multiplying on the right by the vector $\dot{\theta}$ produces the coriolis vector

$$\begin{bmatrix} \frac{4(-2j_1 u\dot{u}^2 - 2j_3 u\dot{u}^2 v^2 + \dot{\gamma}j_3 \dot{v} + \dot{\gamma}j_3 u^2\dot{v} - 4j_1\dot{u}v\dot{v} + 2j_3\dot{u}v\dot{v} + 2j_3 u^2\dot{u}v\dot{v} + \dot{\gamma}j_3 v^2\dot{v} - 2j_3\dot{u}v^3\dot{v} + 2j_1 u\dot{v}^2 - 2j_3 u\dot{v}^2 + 2j_3 uv^2\dot{v}^2)}{(1+u^2+v^2)^3} \\ \frac{4(-(\dot{\gamma}j_3\dot{u}) - \dot{\gamma}j_3 u^2\dot{u} + 2j_1\dot{u}^2 v - 2j_3\dot{u}^2 v + 2j_3 u^2\dot{u}^2 v - \dot{\gamma}j_3\dot{u}v^2 - 4j_1 u\dot{u}\dot{v} + 2j_3 u\dot{u}\dot{v} - 2j_3 u^3\dot{u}\dot{v} + 2j_3 u\dot{u}v^2\dot{v} - 2j_1 v\dot{v}^2 - 2j_3 u^2 v\dot{v}^2)}{(1+u^2+v^2)^3} \\ \frac{4j_3(-(u\dot{u}^2 v) + u^2\dot{u}\dot{v} - \dot{u}v^2\dot{v} + uv\dot{v}^2)}{(1+u^2+v^2)^2} \end{bmatrix} \tag{14}$$

The vector of potential forces is the force from the spring at the spherical joint. The spring resists torsional motion as well as bending motion. The spring model in this analysis assumes that the spring torsional torque is proportional to the angle of the twist, γ. The model also assumes that the torque about the pure bending axis, the axis lying in the UV plane, is proportional to the angle the tool makes with the vertical axis. See Figure 13 for a description of the pure bending axis. This relationship must be transformed into a force in the (u, v) coordinates. Using the equations in (1) and (5), one can show that

$$r := \sqrt{u^2 + v^2} = \frac{\sin(\phi)}{1 + \cos(\phi)}. \tag{15}$$

The spring model assumes that a torque about the pivot axis is proportional to the angle from the vertical axis. In other words,

$$\tau_\phi = K_\phi\phi. \tag{16}$$

The inverse of (15) is

$$\phi = \cos^{-1}\left(\frac{1 - r^2}{1 + r^2}\right). \tag{17}$$

The inverse is obtained by substituting (5) into $\sin(\phi)$ in (15) and then using (2) in the result. The resulting expression is then solved for ϕ. The work done in either system is the same in both coordinate systems. Therefore,

$$K_\phi\,\phi\,d\phi = F_r\,dr.$$

This implies that

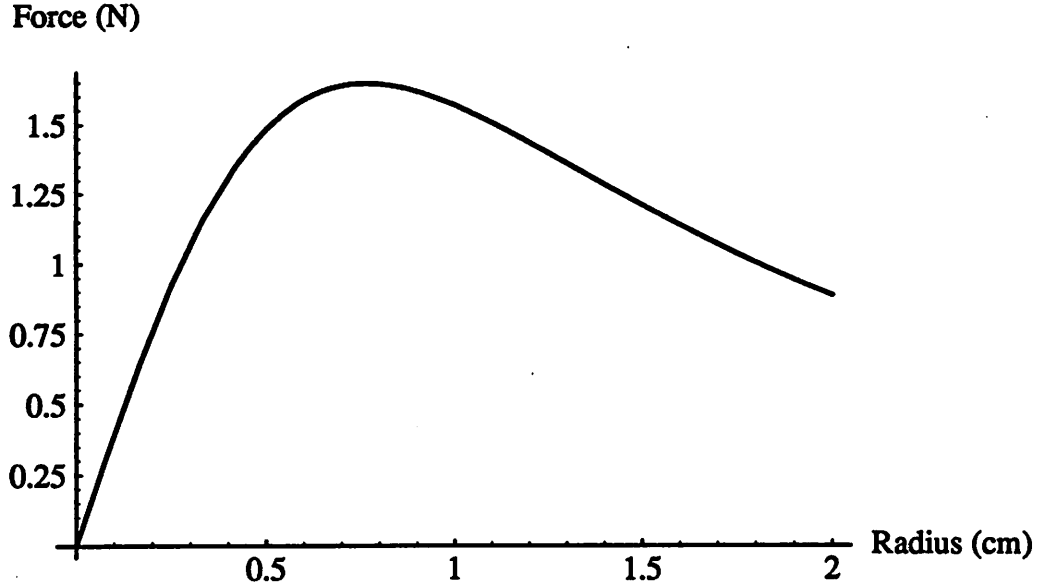$$K_\phi\,\phi\,\frac{d\phi}{dr} = F_r. \tag{18}$$

27

Force (N)

Figure 15: Radial Force

Using (18) and (17) results in the following expression for the radial force

$$F_r = K_\phi \ \cos^{-1} \left(\frac{1 - r^2}{1 + r^2} \right) \frac{2}{1 + r^2}.$$ (19)

The radial force versus r with a value of K_ϕ measured from the prototype is shown in Figure 15. The potential force term in the u and v directions is the radial force projected into these two directions. The complete term is then

$$N(\theta) = \left[\begin{array}{c} F_r(r) \ u/r \\ F_r(r) \ v/r \\ K_\gamma \ \gamma \end{array} \right],$$ (20)

where r is given in (15). One must be careful with this definition when $r = 0$. The force in the u and the v direction is zero when $F_r = 0$. When implementing this model in a controller or in a simulation, one must avoid evaluating this expression near the origin even though the limit exists.

6.4 Control Algorithm

The control algorithm is presented in this section. The relationship between the controller, the platform, and the disturbances is shown in Figure 16. The fact that the system is driven through tendons provides a challenge to design an effective controller. Typically in tendon driven systems, there are more actuators than degrees of freedom. In the endo-platform, there are the same number of degrees of freedom as the number of tendons. In the home

28
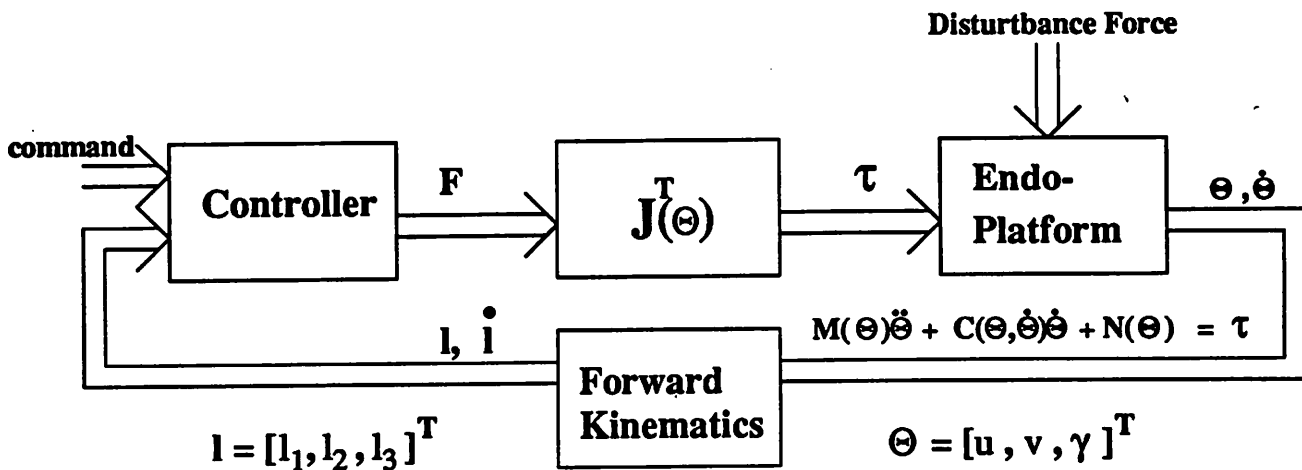
l is the vector of tendon lengths

Θ is the vector of tool frame coordinates

Figure 16: System Block Diagram

configuration, the tendons cannot exert a torque about the twist axis since the bottom row of the jacobian transpose is zero. This leads one to ignore this degree of freedom and control the two coordinates involved in the bending, (u, v). We are then interested in two degrees of freedom and have three actuators that can exert force in only one direction. The control algorithm controls in the workspace coordinates, (u, v), and computes a desired force in these coordinates. The workspace force is then mapped into tendon forces. Forces which lie in the null space of the jacobian transpose are added to provide tension in the three tendons. The forces will affect the torque about the twist axis but the spring in the spherical joint is designed to resist twist. The control algorithm is shown in Figure 17. Since we are ignoring the twist angle in the controller and assume that it is zero for the calculations, the three tendon lengths are dependent. The available information is the length of the tendons and their velocities. This is provided by optical encoders that are attached to the motors which drive the tendons. This information is used to calculate the tool coordinates as well as the velocity of the tool in these coordinates. The inverse kinematics of the platform are solved easily while the forward kinematics are difficult to solve. This also occurs in the Stewart platform. See [13] for more details on the Stewart platform. The equations relating the tool coordinates are nonlinear and difficult to invert. See the equations in the Appendix. The controller numerically solves for the roots of polynomials and produces a vector, $\theta_p := (u, v, 0)^T$. The first two columns of the jacobian are calculated with θ_p. The third column is ignored since we assume that $\gamma = 0$. The new 3×2 jacobian is defined to be $J_p(\theta_p)$. The velocity of the length of the tendons and $J_p^{-1}(\theta_p)$ are used to calculate the velocity in the tool coordinates assuming no twist. This velocity is $\dot{\theta}_p$. This is similar to the method of calculating the velocity in [13]. The velocity and the position
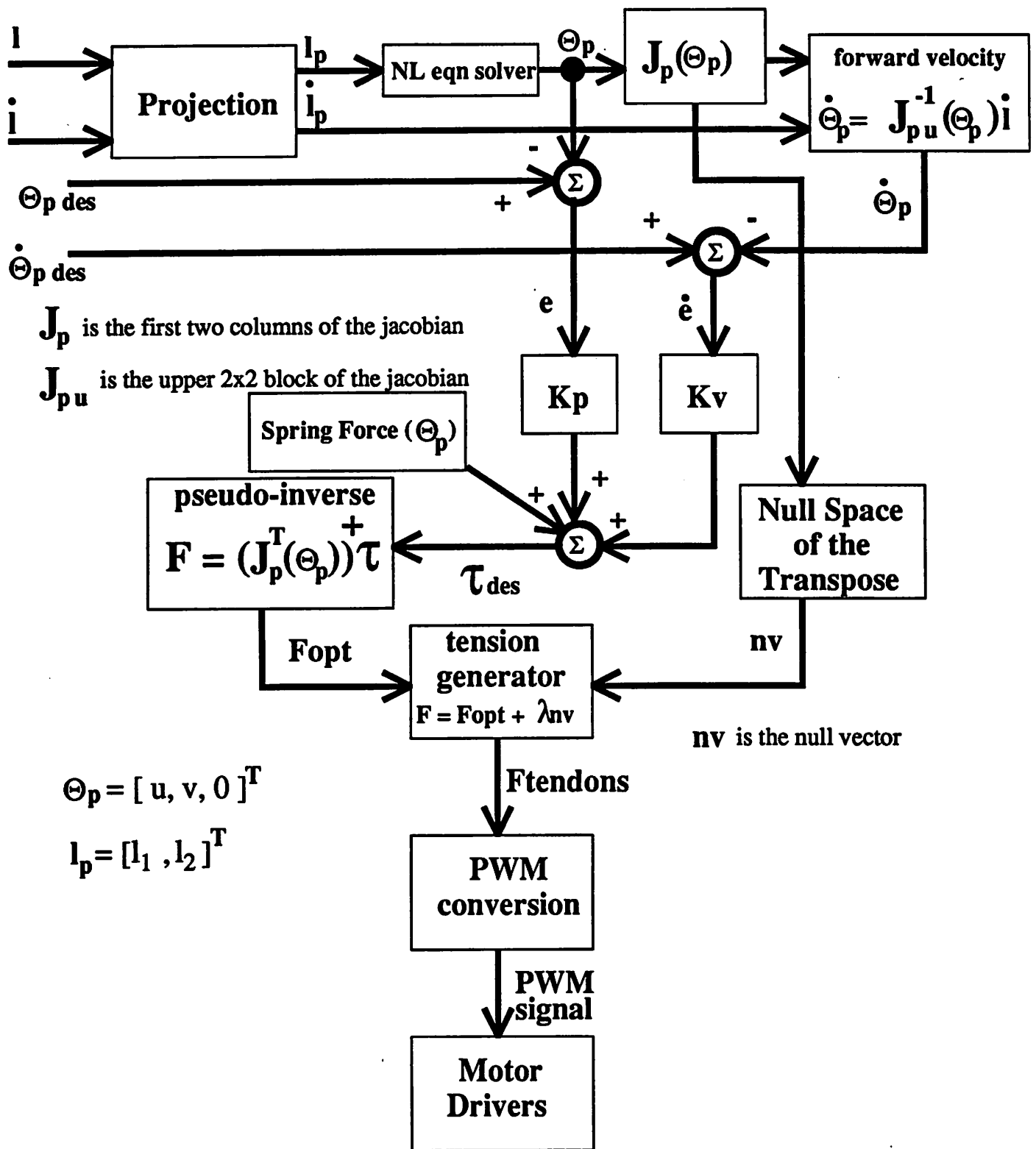
29

Figure 17: Control Algorithm Diagram

information are subtracted from the desired trajectory and an error, $e = \theta_{pdes} - \theta_p$, and error velocity, $\dot{e}$, are formed. The error and error velocity pass through gain matrices to produce a desired torque in the tool coordinates. The spring force in the current configuration is computed and is added to the desired torque from the PD controller. This is a modified PD controller described in [12] however the inertial and Coriolis forces are ignored in this particular controller. The equation for the torque in tool coordinates is

$$\tau = K_p e + K_v \dot{e} + N(\theta_p). \tag{21}$$

The pseudo inverse of $J_p{}^T(\theta_p)$ is used to calculate the optimal force, a force with no component in the null space of $J_p{}^T(\theta_p)$ which maps to τ. The pseudo inverse is denoted $\left(J_p{}^T(\theta_p)\right)^+$. The null space of $J_p{}^T(\theta_p)$ is calculated. The null space is one dimensional, and the null vector is denoted nv. The coefficient, λ, is calculated so that the sum in (22) produces tension forces in the three tendons above a tension offset.

$$F_{tendons} = \left(J_p{}^T(\theta_p)\right)^+ \tau + \lambda\, nv \tag{22}$$

This is the same method described in [4] for producing tendon forces in tension. Tension is a negative force since it decreases the length of the tendon. The desired tendon force is then converted to a pulse width modulated signal to produce a torque in the motors.

This controller subtracts force in the tendons without changing the torque in the tool coordinates. This can always be accomplished if the null space is spanned by a vector with entries with the same sign. Depending on the geometry, this will not occur for certain configurations of the tool. See Figure 18 for cases where one component differs in sign from the other two. In case B in Figure 18, the null vector has a negative first term and the remaining two terms are equal and are positive. A force in the null space corresponds to pushing(pulling) on tendon one and pulling(pushing) on tendon two and three with the same force. In case C in Figure 18, the first component of the null vector is zero and the remaining two components are equal and positive. Any force in tendon one will change the torque in the tool. For the parameters in the prototype, the pointing angle in Case C in Figure 18 is 43.9 degrees. One can conjecture that any pointing angle with respect to the vertical less than this angle results in a null vector having components with the same sign. This has not been proven at this time but is supported by a numerical study of the prototype geometry. The conjecture assumes that $\gamma = 0$. In Figure 19, the null vector components have been plotted as the u and v parameters vary in a circle of radius 0.403 cm. This radius corresponds to the 43.9 degree pointing angle. The components in the null vector remain positive in this range. The parameterized plot in Figure 19 shows that the components remain in the positive quadrant as u and v vary in the circle. One can increase the range where the tendons can exert an arbitrary torque by decreasing the length of dt. The controller without the feed forward term is written in the C programming language and has been tested. The input to the controller is tendon lengths and velocities and the desired position. The output is negative tendon forces. The controller has not been implemented on the prototype but will be implemented in the near future.
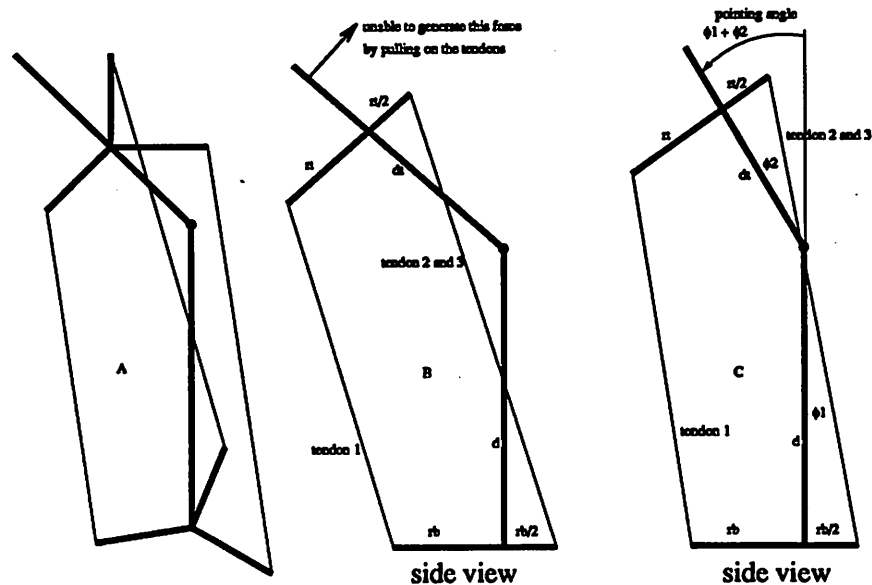
Figure 18: Null Space Geometry

6.5 Simulation Results

The system was simulated in Mathematica [19] with parameters measured from a prototype. The spring model in (20) was used in the controller and in the dynamic model. The current parameters are $d = 1.3$cm, $dt = 0.5$cm, $rt = 0.6$cm, and $rb = 0.6$ cm. The gain matrices are diagonal and have the same coefficient along the diagonal. The kp gain is $26,356g\ cm/(cm\ s^2)$ and kv is $663g\ cm\ s/(cm\ s^2)$. The inertia's were calculated to be $j_1 = j_2 = 2.08g\ cm^2$ and $j_3 = 1.78g\ cm^2$. The spring constants were experimentally determined and are $k_\phi = 100,000g\ cm^2/(s^2\ cm)$ and $k_\gamma = 112,000g\ cm/(s^2\ rad)$. The PD gains were designed in Matlab [11] using the linear quadratic regulator based on the linear error dynamics at the origin. The tool was commanded to step to $u = 0.3$ and $v = 0.2$ from an initial condition close to the origin. The simulated response in position is shown in Figure 20. The response in the UV plane parameterized by time is shown in Figure 21. The closeup of the trajectory is contained in Figure 22. The tension forces in the tendons are shown in Figure 23. Notice the behavior in tendon forces that is similar to the response of non-minimum phase systems. The dip in the tendon forces may be a result of the competing effects of the proportional and derivative terms. The error is positive while the derivative of the error is negative.

The system was also simulated tracking a circle trajectory of radius $0.3cm$ in the UV plane. The frequency of the sines and cosines used to generate the circle is $2Hz$. The endo-platform is initially at the origin and the start point of the trajectory is $(u, v) = (1, 0)$. The resulting trajectory of the tool coordinates in the UV plane is shown in Figure 24. The trajectory of the three tool coordinates over time is shown in Figure 25. The error in the notwist coordinates, $(ud - u, vd - v)$, is shown in Figure 26. Notice that the error does not go to zero but fluctuates around the origin. This cause may be due to the fact that the
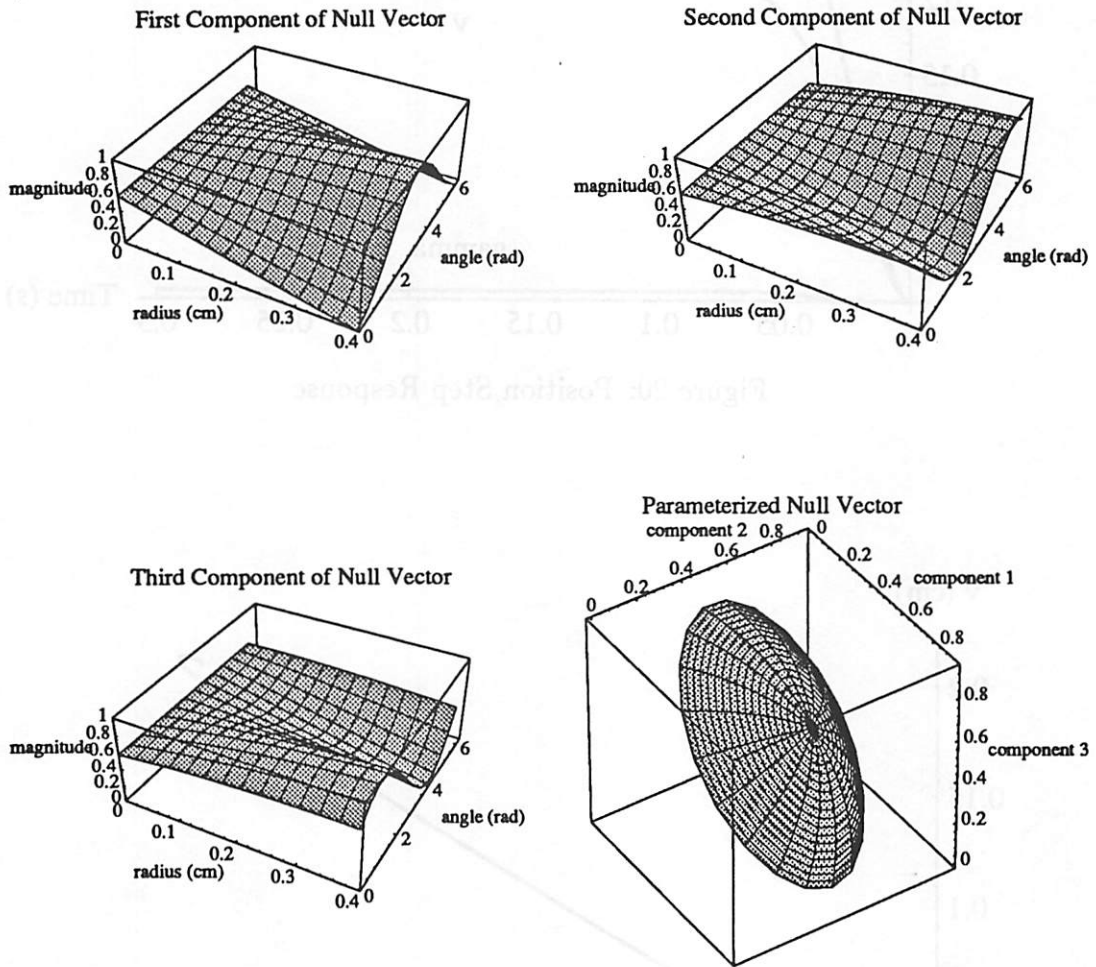
32

First Component of Null Vector

Second Component of Null Vector

Third Component of Null Vector

Parameterized Null Vector

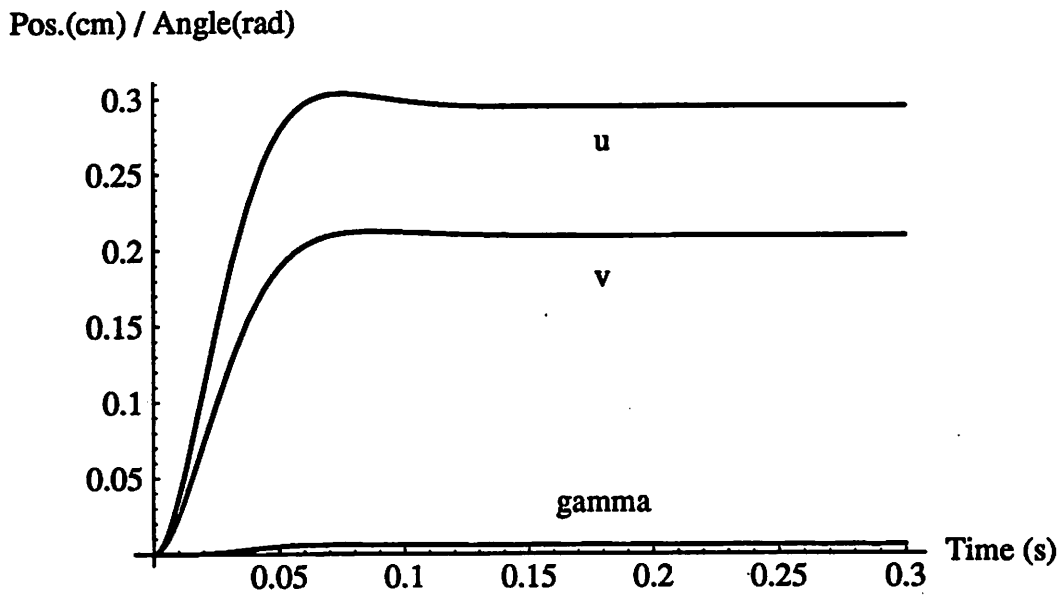Figure 19: Null Vector Components

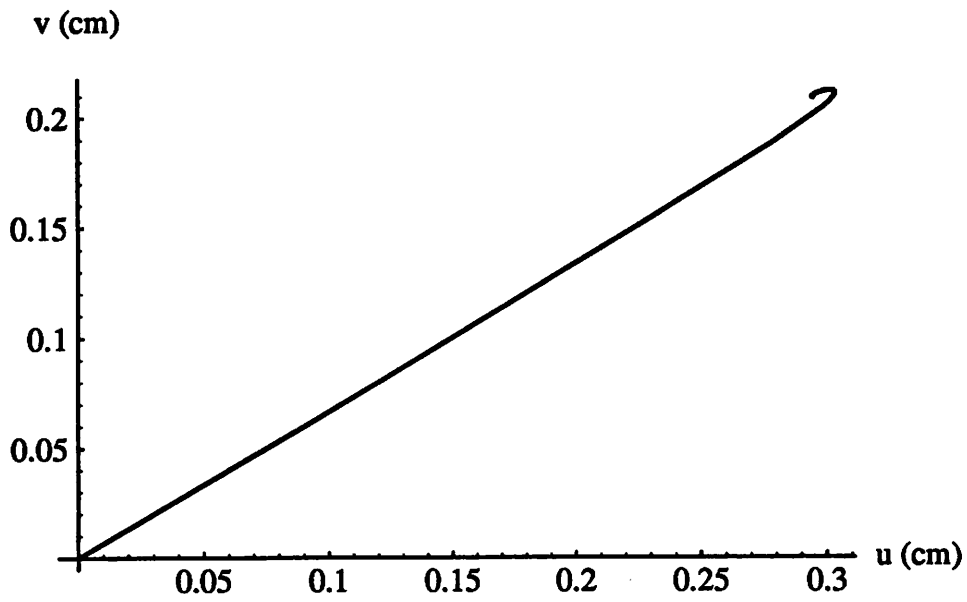Pos.(cm) / Angle(rad)

Figure 20: Position Step Response

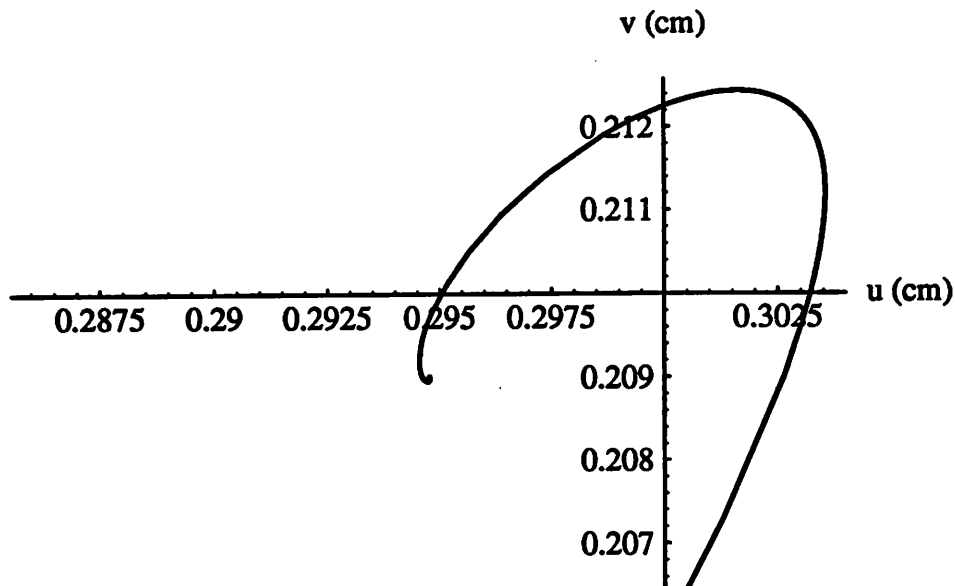Figure 21: Position Step Response

Figure 22: Position Step Response

endo-platform twists, i.e. $\gamma \neq 0$. This is seen in Figure 27. Figure 28 through Figure 30 are the forces in the three tendons over time. Notice that the forces in the tendons are not time shifted copies of the same plot. For example, the maximum force in tendon A is greater than the maximum force in tendon B and C. The tendons are labeled as in Figure 12. The lack of symmetry in the tendon forces may be a result of the nonzero twist angle. The nonzero twist angle effects the jacobian that relates tendon forces to the force experienced in the tool frame. This effects the motion of the platform which effects the errors used in the controller that generates the tendon forces.

6.6 Hardware

A prototype device was created. The outer dimensions of the top and bottom plates are 19 mm. The length of the device is less than 20 mm. Two pictures of the device are shown in Figure 31 and in Figure 32. The three tendons are attached to pulleys on three Maxon DC motors. The motors have optical encoders to read tendon lengths. The control algorithm has not been tested on the device however open loop control has been implemented. The motor forces were commanded directly to position the tool. The endo-platform was capable of 90 degree bends from the vertical axis. The closed loop control will be implemented in the near future.
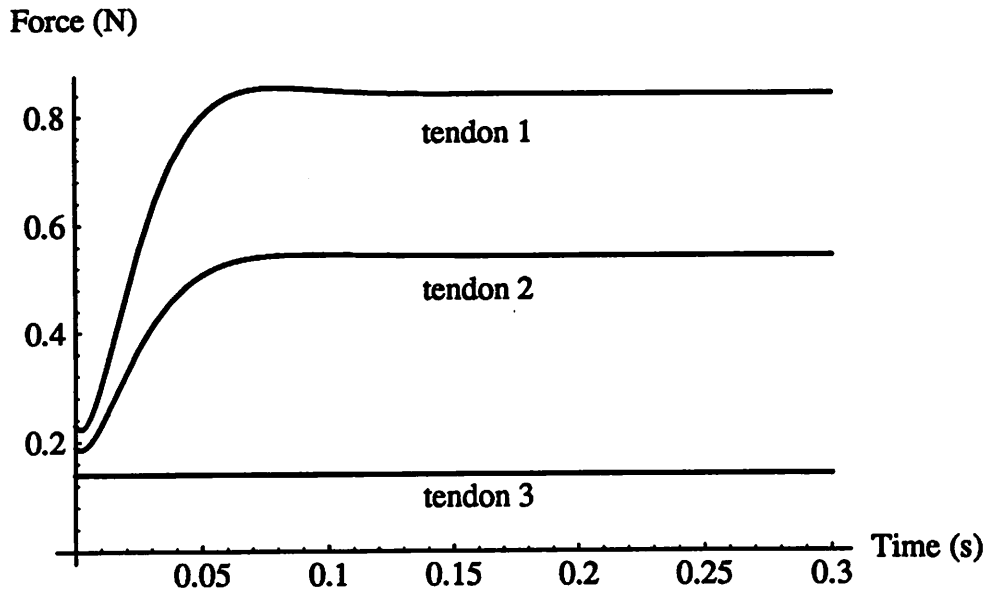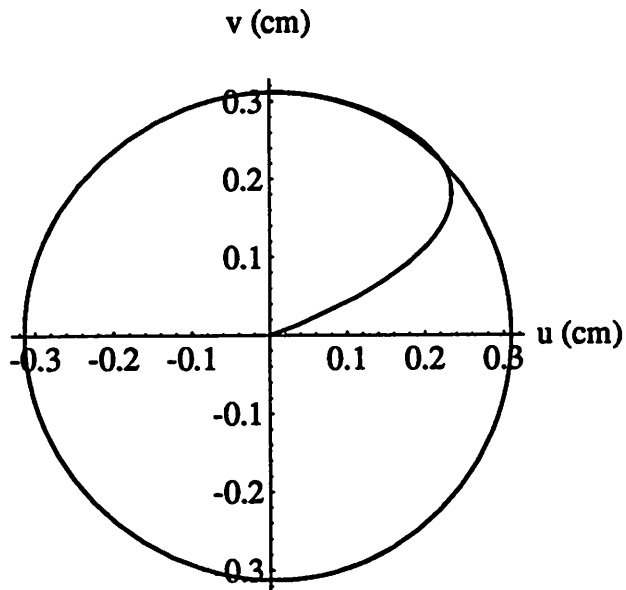
Figure 23: Tendon Force Step Response

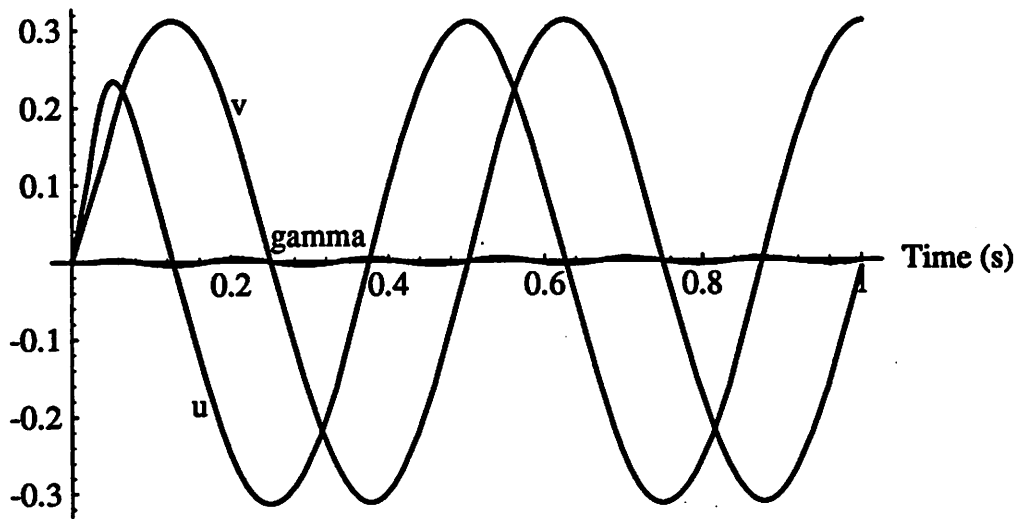Figure 24: Circle Trajectory

36

pos. (cm) & ang. (rad)

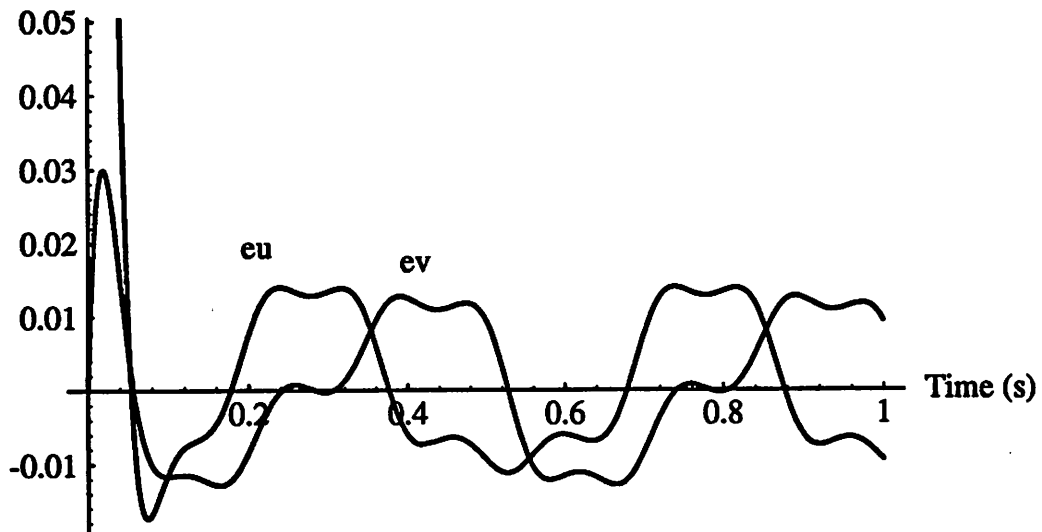Figure 25: Position and Angle Response to Circle Trajectory

error (cm)
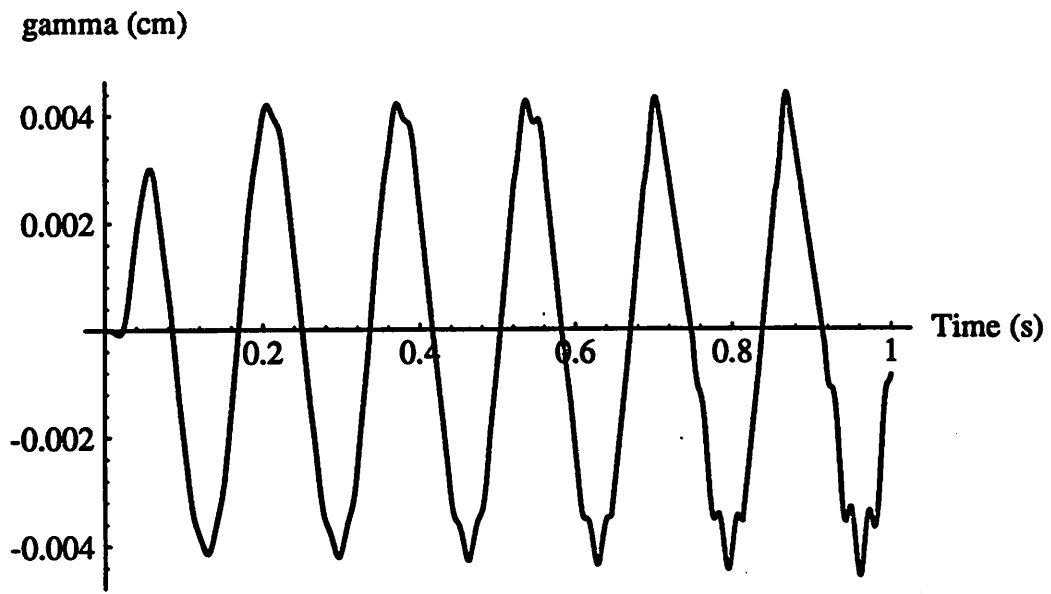

Figure 26: Error Response to Circle Trajectory

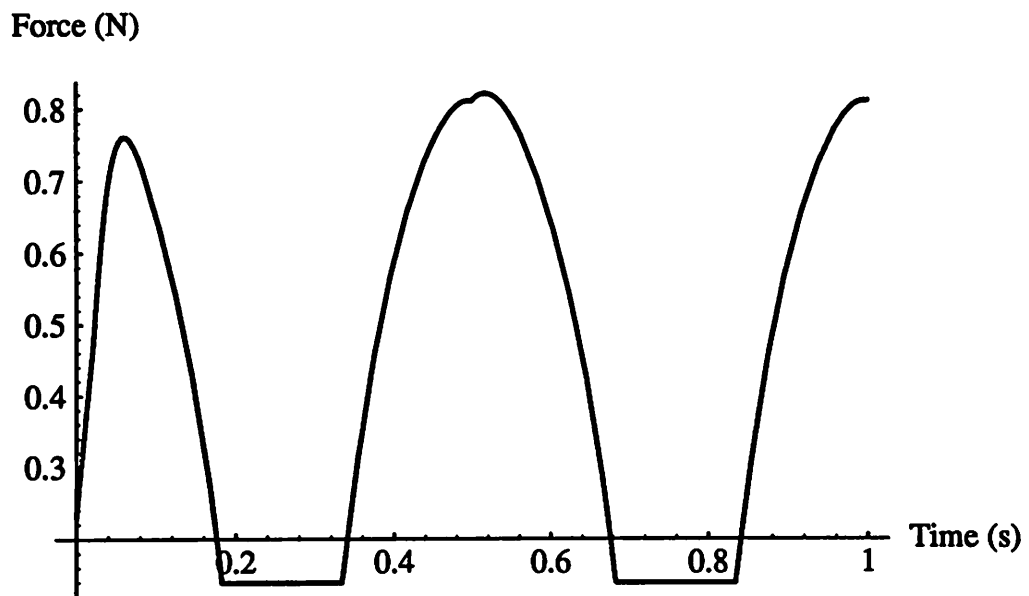Figure 27: Twist Angle Response to Circle Trajectory

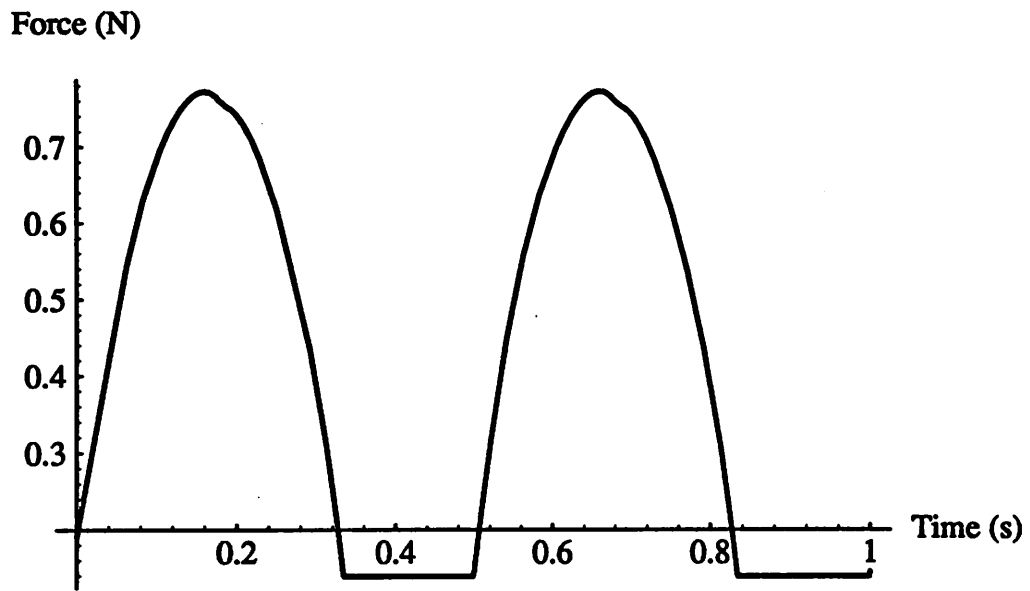Figure 28: Force in Tendon A for Circle Trajectory
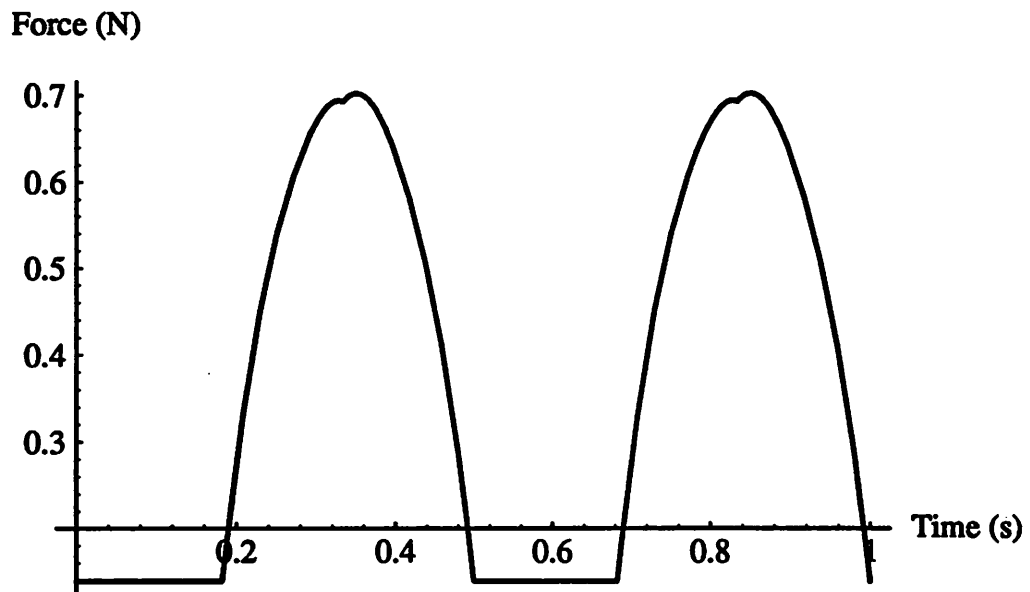
Figure 29: Force in Tendon B for Circle Trajectory

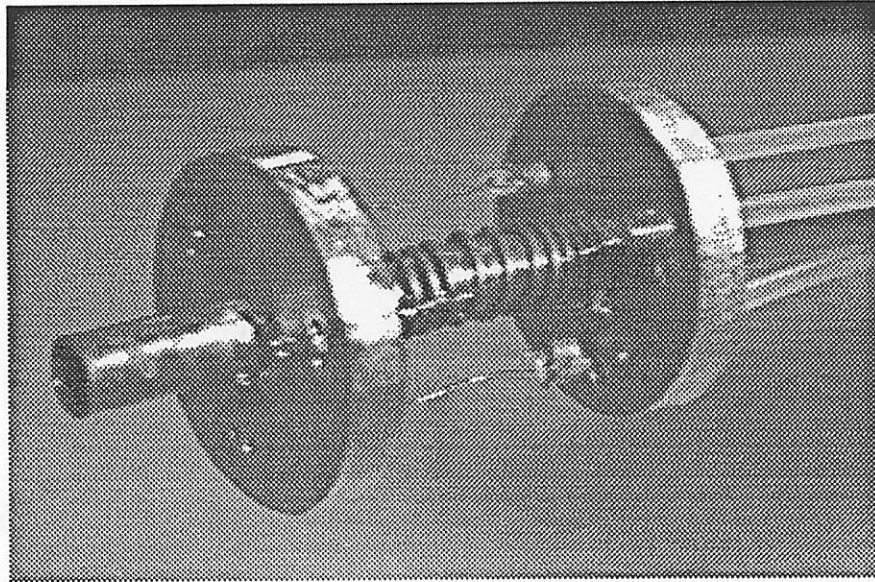Figure 30: Force in Tendon C for Circle Trajectory
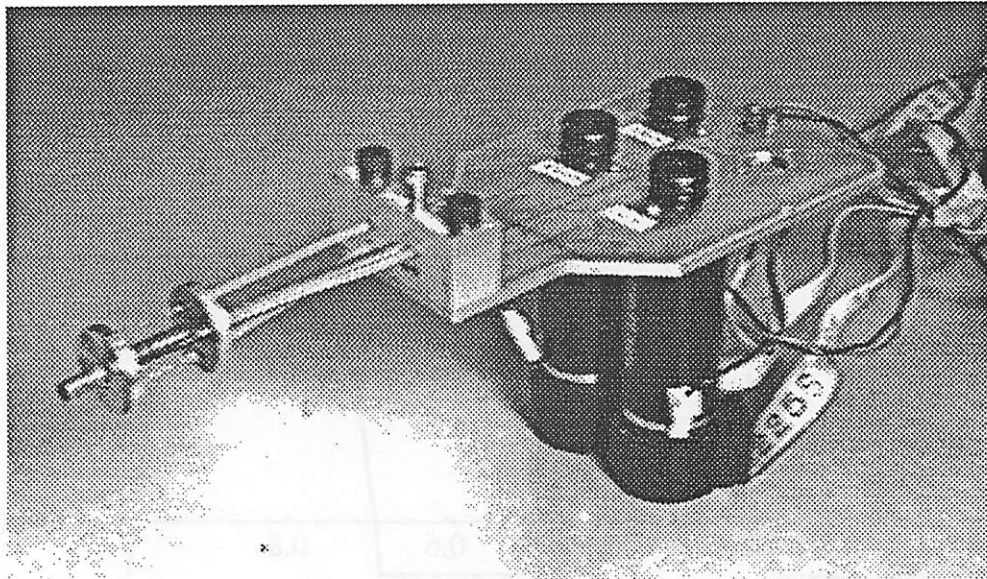
Figure 31: Endo-Platform

Figure 32: Endo-Platform and the Tendon Drivers

7 Conclusion

The report addressed current limitations of endoscopy and proposed designs to expand endoscopes versatility, usefulness, and effectiveness. The fundamental issue as expressed by the author is the lack of fine motion control in current instruments. The hope is that by providing more dexterity, the operations will become more efficient, accurate, and more flexible. Further development of the tools is necessary to provide evidence for the claim. The designs are still preliminary and require further research to expose their limitations and benefits. The endo-platform needs to incorporate the water channels, the light sources, and the video chips. This work has not been accomplished at this time. The tendons for the endo-platform need to be as long as the endoscope length. The effect of the tendon lengths is not known at this time and needs to be investigated further. The endo-platform prototype demonstrated one of the concept designs and a mathematical analysis uncovered more detail and peculiarities of the device. Further analysis may bring more insights into the function of the platform. With further development, the simple designs presented here may result in useful contributions to endoscopy and minimally invasive surgery.

8 Acknowledgements

A   Tendon Length Function and the Jacobian

The geometric parameters in the following equations are d, dt, rt, and rb. The tool coordinates are $\theta = (u, v, \gamma)$, and $t = \frac{2}{1+u^2+v^2}$ in the following equations. The three equations for the tendon lengths are

$$
\begin{aligned}
l_1 = &\ ((d^2 + 2\,d\,dt + dt^2 + rb^2 + rt^2 - 4\,dt\,rb\,u + d^2\,u^2 - 2\,d\,dt\,u^2 + dt^2\,u^2 \\
&+ rb^2\,u^2 + rt^2\,u^2 + d^2\,v^2 - 2\,d\,dt\,v^2 + dt^2\,v^2 + rb^2\,v^2 + rt^2\,v^2 \\
&- 2\,rb\,rt\,\cos(\gamma) - 4\,d\,rt\,u\,\cos(\gamma) + 2\,rb\,rt\,u^2\,\cos(\gamma) - 2\,rb\,rt\,v^2\,\cos(\gamma) \\
&- 4\,d\,rt\,v\,\sin(\gamma) + 4\,rb\,rt\,u\,v\,\sin(\gamma))\,\frac{t}{2}\,)^{1/2}
\end{aligned}
$$

$$
\begin{aligned}
l_2 = &\ ((d^2 + 2\,d\,dt + dt^2 + rb^2 + rt^2 + 2\,dt\,rb\,u + d^2\,u^2 - 2\,d\,dt\,u^2 + dt^2\,u^2 \\
&+ rb^2\,u^2 + rt^2\,u^2 - 2\,\sqrt{3}\,dt\,rb\,v + d^2\,v^2 - 2\,d\,dt\,v^2 + dt^2\,v^2 + rb^2\,v^2 + rt^2\,v^2 \\
&- 2\,rb\,rt\,\cos(\gamma) + 2\,d\,rt\,u\,\cos(\gamma) - rb\,rt\,u^2\,\cos(\gamma) - 2\,\sqrt{3}\,d\,rt\,v\,\cos(\gamma) \\
&- 2\,\sqrt{3}\,rb\,rt\,u\,v\,\cos(\gamma) + rb\,rt\,v^2\,\cos(\gamma) + 2\,\sqrt{3}\,d\,rt\,u\,\sin(\gamma) \\
&+ \sqrt{3}\,rb\,rt\,u^2\,\sin(\gamma) + 2\,d\,rt\,v\,\sin(\gamma) - 2\,rb\,rt\,u\,v\,\sin(\gamma) \\
&- \sqrt{3}\,rb\,rt\,v^2\,\sin(\gamma))\,\frac{t}{2}\,)^{1/2}
\end{aligned}
$$

$$
\begin{aligned}
l_3 = &\ ((d^2 + 2\,d\,dt + dt^2 + rb^2 + rt^2 + 2\,dt\,rb\,u + d^2\,u^2 - 2\,d\,dt\,u^2 + dt^2\,u^2 \\
&+ rb^2\,u^2 + rt^2\,u^2 + 2\,\sqrt{3}\,dt\,rb\,v + d^2\,v^2 - 2\,d\,dt\,v^2 + dt^2\,v^2 + rb^2\,v^2 + rt^2\,v^2 \\
&- 2\,rb\,rt\,\cos(\gamma) + 2\,d\,rt\,u\,\cos(\gamma) - rb\,rt\,u^2\,\cos(\gamma) + 2\,\sqrt{3}\,d\,rt\,v\,\cos(\gamma) \\
&+ 2\,\sqrt{3}\,rb\,rt\,u\,v\,\cos(\gamma) + rb\,rt\,v^2\,\cos(\gamma) - 2\,\sqrt{3}\,d\,rt\,u\,\sin(\gamma) \\
&- \sqrt{3}\,rb\,rt\,u^2\,\sin(\gamma) + 2\,d\,rt\,v\,\sin(\gamma) - 2\,rb\,rt\,u\,v\,\sin(\gamma) \\
&+ \sqrt{3}\,rb\,rt\,v^2\,\sin(\gamma))\,\frac{t}{2}\,)^{1/2}.
\end{aligned}
$$

The equations for the nine elements in the jacobian, $\frac{\partial l}{\partial \theta}$, are

$$
\begin{aligned}
j_{11} = &\ (-(dt\,rb) - 2\,d\,dt\,u + dt\,rb\,u^2 - dt\,rb\,v^2 - d\,rt\,\cos(\gamma) \\
&+ 2\,rb\,rt\,u\,\cos(\gamma) + d\,rt\,u^2\,\cos(\gamma) - d\,rt\,v^2\,\cos(\gamma) + 2\,rb\,rt\,u\,v^2\,\cos(\gamma)
\end{aligned}
$$

$$+ rbrt\,v\,\sin(\gamma) + 2\,drt\,u\,v\,\sin(\gamma) - rbrt\,u^2\,v\,\sin(\gamma) + rbrt\,v^3\,\sin(\gamma))\,t^2\,/(2\,l_1)$$

$$j_{12} = ((-d + rb\,u)\,(2\,dt\,v - 2\,rt\,u\,v\,\cos(\gamma) + rt\,\sin(\gamma) + rt\,u^2\,\sin(\gamma)$$
$$- rt\,v^2\,\sin(\gamma))\,t^2\,/(2\,l_1)$$

$$j_{13} = (rt\,(-2\,d\,v\,\cos(\gamma) + 2\,rb\,u\,v\,\cos(\gamma) + rb\,\sin(\gamma) + 2\,d\,u\,\sin(\gamma) - rb\,u^2\,\sin(\gamma)$$
$$+ rb\,v^2\,\sin(\gamma)))\,t\,/(2\,l_1)$$

$$j_{21} = (dt\,rb - 4\,d\,dt\,u - dt\,rb\,u^2 + 2\sqrt{3}\,dt\,rb\,u\,v + dt\,rb\,v^2 + drt\,\cos(\gamma) + rbrt\,u\,\cos(\gamma)$$
$$- drt\,u^2\,\cos(\gamma) - \sqrt{3}\,rbrt\,v\,\cos(\gamma) + 2\sqrt{3}\,drt\,u\,v\,\cos(\gamma) + \sqrt{3}\,rbrt\,u^2\,v\,\cos(\gamma)$$
$$+ drt\,v^2\,\cos(\gamma) - 2\,rbrt\,u\,v^2\,\cos(\gamma) - \sqrt{3}\,rbrt\,v^3\,\cos(\gamma) + \sqrt{3}\,drt\,\sin(\gamma)$$
$$+ \sqrt{3}\,rbrt\,u\,\sin(\gamma) - \sqrt{3}\,drt\,u^2\,\sin(\gamma) - rbrt\,v\,\sin(\gamma) - 2\,drt\,u\,v\,\sin(\gamma)$$
$$+ rbrt\,u^2\,v\,\sin(\gamma) + \sqrt{3}\,drt\,v^2\,\sin(\gamma) + 2\sqrt{3}\,rbrt\,u\,v^2\,\sin(\gamma)$$
$$- rbrt\,v^3\,\sin(\gamma))\,t^2\,/(4\,l_2)$$

$$j_{22} = -(\sqrt{3}\,dt\,rb) - \sqrt{3}\,dt\,rb\,u^2 - 4\,d\,dt\,v - 2\,dt\,rb\,u\,v + \sqrt{3}\,dt\,rb\,v^2 - \sqrt{3}\,drt\,\cos(\gamma)$$
$$- \sqrt{3}\,rbrt\,u\,\cos(\gamma) - \sqrt{3}\,drt\,u^2\,\cos(\gamma) - \sqrt{3}\,rbrt\,u^3\,\cos(\gamma) + 3\,rbrt\,v\,\cos(\gamma)$$
$$- 2\,drt\,u\,v\,\cos(\gamma) + 2\,rbrt\,u^2\,v\,\cos(\gamma) + \sqrt{3}\,drt\,v^2\,\cos(\gamma) + \sqrt{3}\,rbrt\,u\,v^2\,\cos(\gamma)$$
$$+ drt\,\sin(\gamma) - rbrt\,u\,\sin(\gamma) + drt\,u^2\,\sin(\gamma) - rbrt\,u^3\,\sin(\gamma)$$
$$- \sqrt{3}\,rbrt\,v\,\sin(\gamma) - 2\sqrt{3}\,drt\,u\,v\,\sin(\gamma) - 2\sqrt{3}\,rbrt\,u^2\,v\,\sin(\gamma) - drt\,v^2\,\sin(\gamma)$$
$$+ rbrt\,u\,v^2\,\sin(\gamma))\,t^2\,/(4\,l_2)$$

$$j_{23} = (rt\,(2\sqrt{3}\,d\,u\,\cos(\gamma) + \sqrt{3}\,rb\,u^2\,\cos(\gamma) + 2\,d\,v\,\cos(\gamma) - 2\,rb\,u\,v\,\cos(\gamma)$$
$$- \sqrt{3}\,rb\,v^2\,\cos(\gamma) + 2\,rb\,\sin(\gamma) - 2\,d\,u\,\sin(\gamma) + rb\,u^2\,\sin(\gamma)$$
$$+ 2\sqrt{3}\,d\,v\,\sin(\gamma) + 2\sqrt{3}\,rb\,u\,v\,\sin(\gamma) - rb\,v^2\,\sin(\gamma)))\,t\,/(4\,l_2)$$

$$j_{31} = (dt\,rb - 4\,d\,dt\,u - dt\,rb\,u^2 - 2\sqrt{3}\,dt\,rb\,u\,v + dt\,rb\,v^2 + drt\,\cos(\gamma) + rbrt\,u\,\cos(\gamma)$$
$$- drt\,u^2\,\cos(\gamma) + \sqrt{3}\,rbrt\,v\,\cos(\gamma) - 2\sqrt{3}\,drt\,u\,v\,\cos(\gamma) - \sqrt{3}\,rbrt\,u^2\,v\,\cos(\gamma)$$
$$+ drt\,v^2\,\cos(\gamma) - 2\,rbrt\,u\,v^2\,\cos(\gamma) + \sqrt{3}\,rbrt\,v^3\,\cos(\gamma) - \sqrt{3}\,drt\,\sin(\gamma)$$
$$- \sqrt{3}\,rbrt\,u\,\sin(\gamma) + \sqrt{3}\,drt\,u^2\,\sin(\gamma) - rbrt\,v\,\sin(\gamma) - 2\,drt\,u\,v\,\sin(\gamma)$$
$$+ rbrt\,u^2\,v\,\sin(\gamma) - \sqrt{3}\,drt\,v^2\,\sin(\gamma) - 2\sqrt{3}\,rbrt\,u\,v^2\,\sin(\gamma)$$
$$- rbrt\,v^3\,\sin(\gamma))\,t^2\,/(4\,l_3)$$

$$j_{32} = (\sqrt{3}\,dt\,rb + \sqrt{3}\,dt\,rb\,u^2 - 4\,d\,dt\,v - 2\,dt\,rb\,u\,v - \sqrt{3}\,dt\,rb\,v^2 + \sqrt{3}\,drt\,\cos(\gamma)$$

$$+\sqrt{3}\,rbrt\,u\,\cos(\gamma) + \sqrt{3}\,drt\,u^2\,\cos(\gamma) + \sqrt{3}\,rbrt\,u^3\,\cos(\gamma) + 3\,rbrt\,v\,\cos(\gamma)$$
$$-2\,drt\,u\,v\,\cos(\gamma) + 2\,rbrt\,u^2\,v\,\cos(\gamma) - \sqrt{3}\,drt\,v^2\,\cos(\gamma) - \sqrt{3}\,rbrt\,u\,v^2\,\cos(\gamma)$$
$$+drt\,\sin(\gamma) - rbrt\,u\,\sin(\gamma) + drt\,u^2\,\sin(\gamma) - rbrt\,u^3\,\sin(\gamma)$$
$$+\sqrt{3}\,rbrt\,v\,\sin(\gamma) + 2\sqrt{3}\,drt\,u\,v\,\sin(\gamma) + 2\sqrt{3}\,rbrt\,u^2\,v\,\sin(\gamma)$$
$$-drt\,v^2\,\sin(\gamma) + rbrt\,u\,v^2\,\sin(\gamma))\,t^2\,/(4\,l_3)$$

$$j_{33} = (rt\,(-2\sqrt{3}\,du\,\cos(\gamma) - \sqrt{3}\,rb\,u^2\,\cos(\gamma) + 2\,dv\,\cos(\gamma) - 2\,rb\,u\,v\,\cos(\gamma)$$
$$+\sqrt{3}\,rb\,v^2\,\cos(\gamma) + 2\,rb\,\sin(\gamma) - 2\,du\,\sin(\gamma) + rb\,u^2\,\sin(\gamma)$$
$$-2\sqrt{3}\,dv\,\sin(\gamma) - 2\sqrt{3}\,rb\,u\,v\,\sin(\gamma) - rb\,v^2\,\sin(\gamma)))\,t\,/(4\,l_3).$$

References

[1] John Baillie. *Gastrointestinal Endoscopy: Basic Principles and Practice.* Butterworth-Heinemann, Oxford, 1992.

[2] M. Cohn, C. Deno, and J. Fuji. Hydraulic actuator, robot containing same, and method of producing same, 1993.

[3] M Cremer, J Deviere, M Baize, and C Matos. New device for endoscopic cystoenterostomy. *Endoscopy*, 22(2):394–398, Mar 1990.

[4] C. Deno, R. Murray, K. Pister, and S. Sastry. Finger-like biomechanical robots. Erl technical report, University of California at Berkeley, 1992. Department of EECS.

[5] D. C. Deno. *Control Theoretic Investigations of the Visual Smooth Pursuit System.* PhD thesis, U.C. Berkeley, 1991.

[6] J Escourro, M Delvaux, L Buscall, R Darmana, J Frexinos, JP Morucci, and A Ribiet. First clinical evaluation and experimental study of a new mechanical suture device for endoscopic hemostasis. *Gastrointestinal Endoscopy*, 36(5):494–497, Sep-Oct 1990.

[7] J. Funda and R.P. Paul. A comparison of transforms and quaternions in robotics. In *IEEE International Conference on Robotics and Automation*, Philadelphia, 1988.

[8] S. Hirose. *Biologically Inspired Robots: Snake-Like Locomotors and Manipulators.* Oxford University Press, Oxford, 1993.

[9] K. Ikuta, M. Tsukamoto, and S. Hirose. Shape memory alloy servo actuator system with electric resistance feedback and application for active endoscope. In *IEEE International Conference on Robotics and Automation*, Philadelphia, 1988.

[10] K. Knyrim, H. Seidlitz, N. Vakil, and M. Classen. Perspectives in "electronic endoscopy". past, present and future of fibers and ccd's in medical endoscopes. *Endoscopy*, 22(Suppl 1):2–8, Sep 1990.

[11] MathWorks, Natick, Ma. *Matlab Reference Guide*, 1992.

[12] R. Murray, Z. Li, and S. Sastry. *A Mathematical Introduction to Robotic Manipulation*. Preprint, 1993.

[13] C. Nguyen, Z. Zhou, S. Antranzi, and C. Campbell. Efficient computation of forward kinematics and jacobian matrix of a stewart platform-based manipulator. In *IEEE Proceedings of SOUTHEASTCON*, Williamsburg, Va., 1991.

[14] Christopher Rall, M.D. and James Richter, M.D. Personal Communication at Massachusetts General Hospital, November 1992.

[15] Jerome H. Siegel. *Endoscopic Retrograde Cholangiopancreatography: Technique, Diagnosis, and Therapy*. Raven Press, New York, 1992.

[16] Fred E. Silverstein and Guido N.J. Tytgat. *Atlas of Gastrointestinal Endoscopy*. Gower Medical, New York, 1991.

[17] R. H. Sturges, Jr. and S. Laowattana. A flexible, tendon-controlled device for endoscopy. *The Inernational Journal of Robotics Research*, 12(2):121–131, Apr 1993.

[18] G. Walsh, R. Montgomery, and S. Sastry. Orientation control of the dynamic satellite. In *To be presented at the 1994 A.C.C*, 1993 preprint.

[19] S. Wolfram. *Mathematica: A System for Doing Mathematics by Computer*. Addison-Wesley, RedWood City, second edition, 1991.